

Gravitational waves from the early universe

Rafael R. Lino dos Santos^{1,2,æ*} and Linda M. van Manen^{3,†}

1 CP3-Origins, University of Southern Denmark, Campusvej 55, DK-5230 Odense M, Denmark

2 University of Münster, Institute for Theoretical Physics, 48149 Münster, Germany

3 Friedrich-Schiller-Universität, Institute for Theoretical Physics, 07743 Jena, Germany

^æ rado@cp3.sdu.dk [†] linda.van.manen@uni-jena.de

December 13, 2022

Abstract

These lecture notes are based on the course "Gravitational waves from the early universe" given at the 27th W.E. Heraeus "Saalburg" Summer School 2021 by Valerie Domcke.

Ongoing and future collaborations will probe different frequency ranges of the gravitational wave spectrum, allowing for probing different stages of the early universe and Beyond Standard Model physics. Due to the very high energies involved, accelerators cannot probe them. Therefore, current knowledge about new physics is limited and relies on bounds from CMB observations and theoretical assumptions about these energy scales. While some models are in tension with CMB data, others are unconstrained in shorter wavelength scales. Nonetheless, each one of these models has a gravitational wave density spectrum that can be compared to data. These lecture notes review the formalism of gravitational waves in General Relativity and introduce stochastic gravitational waves, primordial sources, and detection efforts.

Contents

1	Motivation	2
2	Lecture: Linearized Einstein equations	5
2.1	The linearized Einstein equations	5
2.2	Scalar, vector, tensor (SVT) decomposition	6
2.3	Gauge invariance and gauge fixing	7
2.4	Vacuum solutions	8
2.5	Effects of gravitational waves on test masses	9
3	Lecture: Emission of gravitational waves	10
3.1	Gravitational waves emitted by source	11
3.2	Energy momentum tensor of gravitational waves	13
3.3	Einstein's quadrupole formula	15
4	Lecture: The stochastic gravitational wave background	16
4.1	The gravitational wave background	16
4.2	gravitational waves in expanding FRW universe	17

4.3	Searching for SGWBs	20
4.3.1	Experimental setting	21
4.3.2	Overlap reduction function	22
4.3.3	Monopole response function	22
4.4	Experiments	24
4.4.1	Ground-based interferometers	24
4.4.2	Space-based interferometers	24
4.4.3	Pulsar timing arrays	26
5	Lecture: Cosmological sources - Probing beyond Standard Model physics	26
5.1	Characteristic frequencies of relic gravitational waves	27
5.2	Constraints from BBN and CMB	28
5.3	Cosmic gravitational microwave background	28
5.4	First order phase transitions	28
5.5	Cosmic strings	29
6	Lecture: Gravitational waves from axion inflation	33
6.1	Cosmic inflation	33
6.2	gravitational waves from inflation	34
6.3	Axion inflation	36
7	Conclusions	38
	References	40

1 Motivation

Look far away into the deep abyss of space and see how the first galaxy formed a long time ago. Look further and see the first stars. We can look all the way back to a time when the universe had a temperature of approximately $T \approx eV$, and free electrons for the first time combined with protons to form hydrogen. An event known as recombination¹. After recombination, photons could travel freely through space. Since then, they have been propagating in the universe, occasionally reaching our detectors. The moment when the first photons freely traveled through the universe is known as photon decoupling. These first photons are still visible today as the Cosmic Microwave Background (CMB), a background noise from all directions, easily confused with pigeon poop on the antenna². Before photon decoupling, light could not travel freely through the hot proton-electron plasma making up the young universe. The photons scattered continuously off the electrons and protons in the hot plasma, making the universe opaque. This shrouds everything that happened before photon decoupling in darkness and makes it complicated for physicists

¹The term recombination mainly confuses students about the number of times the event of protons and electrons combining has occurred. This event has, as a matter of fact, occurred only once.

²When Robert W. Wilson and Arno A. Penzias first heard the radio signal, they initially thought it might have been caused by the poop of the pigeons surrounding the radio antenna. Not until they cleaned the antenna of the pigeon poop they realized what they had discovered.

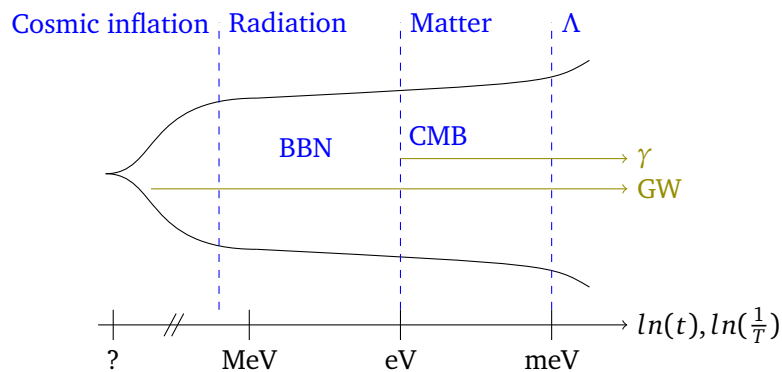


Figure 1: A visualization of our cosmic history. Starting from the big bang on the left, our universe went through an era of cosmic inflation, followed by a radiation-dominated era, a matter-dominated era, and, finally, the current era dominated by dark-energy (cosmological constant Λ), which accelerates the expansion of the universe. The different eras are presented on a timescale given in the horizontal axis by $\ln(\frac{1}{T})$, with T the temperature of the universe, or $\ln(t)$, where t is the time since the Big Bang. The characteristic energy scales of these different eras are also presented on the horizontal axis. The earliest freely moving photons that we can observe today is known as the cosmic microwave background radiation (CMB). The emission of these photons is represented by γ . On the other hand, gravitational waves (GW) from the early universe can be observed from much earlier times. They can be produced as early as cosmic inflation, are expected to transverse the universe largely unperturbed, and are expected to be detected in a few decades, giving important hints for the development of inflation and new physics models.

to observe what happened at the beginning and in the first years of our universe.

However, not all hope is lost with the discovery of gravitational waves. Early universe phenomena could have created gravitational waves. They may have been produced as early as cosmic inflation, creating a background of gravitational waves similar to the CMB, known as the gravitational wave background or stochastic gravitational wave background (SGWB). Unlike photons before decoupling, gravitational waves traveled through the early universe largely unperturbed. Thus, no fundamental obstacle prevents us from observing these early gravitational waves and discovering information about the earlier stages of our universe. Although there are no fundamental obstacles, there are plenty of experimental challenges.

Similar to the CMB, the gravitational wave background is expected to be like noise from all directions. However, the gravitational background noise is far too weak for all our current detectors to measure, and we need to distinguish the gravitational wave background noise from other noise sources. Nonetheless, different collaborations expect to detect the gravitational wave background in the coming years³, and a lot can be learned from early universe gravitational waves. Take, for example, the gravitational wave frequency spectrum. Gravitational waves can come in different frequencies, and each collaboration probes a different spectrum range. Analogous to an orchestra where different instruments are combined, it is possible to combine data from different collaborations in a *gravitational wave orchestra* to get information about different stages of the universe⁴.

Finally, different early universe sources can produce gravitational waves. Inflation and beyond Standard Model (BSM) physics phenomena, such as cosmic strings and first-order phase transitions, are examples. Remarkably, BSM depends on energy scales that are far beyond what accelerators on Earth can probe. Therefore, the gravitational wave background also serves as a laboratory to probe new physics! All this information in the gravitational wave background further completes our knowledge of our cosmic history. The study of gravitational waves from the early universe is part of the answer to a question as old as mankind: *Where do we come from?*

The lectures are organized in the following sequence. In Sec. 2, we obtain gravitational waves as vacuum solutions of the linearized Einstein equations and study the effects of gravitational waves on test masses. Next, in Sec. 3, we study sourced emission of gravitational waves and their energy-momentum tensor and derive Einstein's quadrupole formula for the power emitted by a source. Then, in Sec. 4, we focus on the background of stochastic gravitational waves, derive the main properties, and describe detection efforts. In Sec. 5, we start discussing cosmological sources of gravitational waves (cosmic gravitational microwave background, first-order phase transitions, and cosmic strings) and how data can be used to constrain beyond Standard Model physics. Finally, in Sec. 6, we finish the discussion on cosmological sources with single-field slow-roll inflation and axion inflation.

³Some of these collaborations are already active. They rely on ground-based detectors (LIGO, Virgo, KAGRA) or pulsar time arrays collaborations (NANOGrav, EPTA, PPTA, IPTA). Future collaborations include a space-based detector (LISA) and ground-based detectors (Cosmic Explorer and Einstein telescope).

⁴Following the analogy with the music world, in a string quintet we can go from the double bass (low) to the cello, and then to the viola and the violins (high). Likewise, in the gravitational wave orchestra of the early universe, we can go from matter domination to radiation domination era, then reheating and inflation.

2 Lecture: Linearized Einstein equations

In this first lecture, we start by evaluating linearized general relativity, which describes the dynamics of a slightly perturbed gravitational field. After all, we can think about gravitational waves as *small* ripples in flat spacetime. Hence, we consider a metric tensor decomposed into the Minkowski metric and a small perturbation,

$$g_{\mu\nu} = \eta_{\mu\nu} + h_{\mu\nu}(x), \quad \text{with } |h_{\mu\nu}| \ll 1, \quad (2.1)$$

where higher order in h can be omitted due to the smallness of h . Furthermore, we use the $(-, +, +, +)$ sign notation for $\eta_{\mu\nu}$ and the indices are raised with $\eta_{\mu\nu}$, i.e., $g^{\mu\nu} = \eta^{\mu\nu} - h^{\mu\nu}$. Afterward, we will look into the number of degrees of freedom the metric perturbation contains and discuss the most used gauge for fixing the unphysical degrees of freedom. Lastly, we will solve the Einstein equation for test masses far from the source of gravitational waves. All the material in the first two lectures is based on the book “Gravitational Waves: Volume 1: Theory and Experiments” by Michel Maggiore [1] and “Spacetime and Geometry. An introduction to general relativity” by Sean Carroll [2]. We recommend these references for an elaborate and detailed explanation of linearized general relativity and gravitational waves.

2.1 The linearized Einstein equations

The familiar Einsteins equations are given by,

$$G_{\mu\nu} \equiv R_{\mu\nu} - \frac{1}{2}g_{\mu\nu}R = \frac{8\pi G}{c^4}T_{\mu\nu}, \quad (2.2)$$

which relates the spacetime geometry, encoded in the metric $g_{\mu\nu}$, to matter described by the energy-momentum tensor $T_{\mu\nu}$. The Ricci tensor $R_{\mu\nu}$ and Ricci scalar R for the linearized theory are computed following the usual scheme, starting from the Christoffel symbol. One can easily check that the linearized Christoffel symbol is given by

$$\begin{aligned} \Gamma_{\mu\nu}^{\rho} &= \frac{1}{2}g^{\rho\sigma}[\partial_{\mu}g_{\nu\sigma} + \partial_{\nu}g_{\mu\sigma} - \partial_{\sigma}g_{\mu\nu}] \\ &= \frac{1}{2}\eta^{\rho\sigma}[\partial_{\mu}h_{\nu\sigma} + \partial_{\nu}h_{\mu\sigma} - \partial_{\sigma}h_{\mu\nu}] + \mathcal{O}(h^2), \end{aligned} \quad (2.3)$$

which leads to the following Riemann curvature tensor,

$$\begin{aligned} R_{\nu\sigma\rho}^{\mu} &= \partial_{\sigma}\Gamma_{\nu\rho}^{\mu} - \partial_{\rho}\Gamma_{\nu\sigma}^{\mu} + \Gamma_{\sigma\lambda}^{\mu}\Gamma_{\nu\rho}^{\lambda} - \Gamma_{\rho\lambda}^{\mu}\Gamma_{\nu\sigma}^{\lambda} \\ &= \frac{1}{2}[\eta^{\mu\lambda}(\partial_{\sigma}\partial_{\nu}h_{\rho\lambda} - \partial_{\sigma}\partial_{\rho}h_{\nu\lambda} - \partial_{\sigma}\partial_{\lambda}h_{\nu\rho} - (\sigma \leftrightarrow \rho))] + \mathcal{O}(h^2). \end{aligned} \quad (2.4)$$

Note that the Γ^2 terms are higher-order terms in h and will not contribute to the first-order Einstein equations. With a bit of algebra, one can then find the Ricci tensor,

$$R_{\mu\nu} = R_{\mu\rho\nu}^{\rho} = \frac{1}{2}(\partial_{\rho}\partial_{\mu}h_{\nu}^{\rho} + \partial_{\rho}\partial_{\nu}h_{\mu}^{\rho} - \partial_{\mu}\partial_{\nu}h - \square h_{\mu\nu}) + \mathcal{O}(h^2), \quad (2.5)$$

and the Ricci scalar

$$R = g^{\mu\nu}R_{\mu\nu} = \partial_\mu\partial_\nu h^{\mu\nu} - \square h + \mathcal{O}(h^2), \quad (2.6)$$

with $h = h^\mu{}_\mu$ the trace and $\square = \partial_\mu\partial^\mu$. Combining all the results gives us the linearized Einstein tensor

$$G_{\mu\nu} = \frac{-1}{2}[\square h_{\mu\nu} + \eta_{\mu\nu}\partial^\rho\partial^\sigma h_{\rho\sigma} - \eta_{\mu\nu}\square h - \partial^\rho\partial_\nu h_{\mu\rho} - \partial_\rho\partial_\mu h_\nu{}^\rho + \partial_\nu\partial_\mu h] + \mathcal{O}(h^2). \quad (2.7)$$

This is a rather lengthy equation; hence it is usually preferred to define the trace reversed quantity $\bar{h}_{\mu\nu} \equiv h_{\mu\nu} - \frac{1}{2}\eta_{\mu\nu}h$. This simplifies the equation a little to

$$G_{\mu\nu} = \frac{-1}{2}[\square\bar{h}_{\mu\nu} + \eta_{\mu\nu}\partial^\rho\partial^\sigma\bar{h}_{\rho\sigma} - \partial^\rho\partial_\nu\bar{h}_{\mu\rho} - \partial_\rho\partial_\mu\bar{h}_{\nu\rho}] + \mathcal{O}(h^2). \quad (2.8)$$

2.2 Scalar, vector, tensor (SVT) decomposition

General relativity is invariant under all coordinate transformations. The linearized theory, however, is only invariant under infinitesimal coordinate transformations and finite, global Poincaré transformations. In order to study particular physical quantities, it is useful to fix a gauge to eliminate the redundancies due to symmetry under these coordinate transformations. It is convenient to choose a fixed inertial coordinate system on the Minkowski background because the Minkowski background has a lot of rotational symmetries [2]. Hence, this allows us to decompose the perturbation based on their transformation under *spatial* rotations on a hypersurface. Under these spatial rotations, the metric perturbation can be decomposed into scalars, vectors, and tensors, which transform independently from each other. This allows us to write the Einstein equations for the *linearized theory* as a set of uncoupled ordinary differential equations.

On a side note, in the field of cosmology, the SVT decomposition is not uncommonly described in Fourier space⁵. The different Fourier modes in our linear theory are independent of each other. This is due to the translation invariance of the linear equation of motion of the perturbation [3]. Hence, they can be studied independently. Consider the rotations of the coordinate system around a single wavevector \vec{k} by an angle ψ . A perturbation with a helicity m has its amplitude multiplied by $e^{im\psi}$. The perturbations are then classified according to their helicity m . The scalar, vector, and tensor are defined by $m = 0, \pm 1$, and ± 2 , respectively.

Let us have a closer look at the SVT decomposition. The metric perturbation is a $(0, 2)$ tensor with a spatial $SO(3)$ symmetry. Under these rotations, the h_{00} component is a scalar, h_{0i} is a three-vector, and h_{ij} is a spatial rank 2 symmetric tensor [2]. This tensor can further be decomposed into a trace and a trace-free part. In group theory language, these are the irreducible representations of the spatial rotation group. For the metric $g_{\mu\nu}$, decomposed as

$$g_{\mu\nu} = \begin{pmatrix} g_{00} & | & g_{0i} \\ g_{i0} & | & g_{ij} \end{pmatrix},$$

⁵Note that the wavevector defines a direction of propagation which breaks the spatial $SO(3)$ symmetry of the perturbation tensor in a spatial $SO(2)$ symmetry.

the irreducible parts with respect to spatial rotations are then given by

$$\begin{aligned} g_{00} &= -(1 + 2\Phi), \\ g_{i0} = g_{0i} &= 2a(\partial_i B - S_i), \\ g_{ij} &= a^2[(1 - 2\Psi)\delta_{ij} + 2\partial_{ij}F + (\partial_i T_j + \partial_j T_i) + t_{ij}]. \end{aligned} \quad (2.9)$$

Here, $g_{00} = -1$, and $g_{ij} = a^2\delta_{ij}$ are components of the background metric. The remaining terms are part of the perturbation $h_{\mu\nu}$ consisting of 4 scalars (Φ, B, Ψ, F), 2 vectors (S_i, T_i), and 1 tensor (t_{ij}), with

$$\partial_i T^i = 0, \quad \partial_i S^i = 0, \quad t^i_i = 0, \quad \text{and} \quad \partial_i t^i_j = 0. \quad (2.10)$$

We find 10 independent functions in the decomposed metric. Namely, 4 of the scalars, 4 vector components, and 2 tensor components of the 3×3 symmetric tensor t_{ij} .

2.3 Gauge invariance and gauge fixing

Now, before we can start solving the linearized Einstein equations, we need to address the ambiguous definition of the perturbation $h_{\mu\nu}$. This perturbation may have different forms depending on the choice of coordinate system. Hence, the metric is defined up to a gauge transformation. Indeed, if we consider an infinitesimal gauge transformation $x^\mu = x^\mu + \xi^\mu$, the perturbation transforms as

$$h_{\mu\nu}(x) \rightarrow h'_{\mu\nu}(x') - \partial_\mu \xi_\nu - \partial_\nu \xi_\mu, \quad (2.11)$$

where ξ is small such that the conditions for a linearized theory, $|h_{\mu\nu}| \ll 1$, is preserved. In general, the vector ξ can be written in terms of two scalars and one vector, $\xi^\mu = (\xi^0, \partial_i f + f_i)$, with $\partial_i f^i = 0$ [1]. Consequently, two scalars and one vector can be gauged away by fixing ξ . This reduces the scalar with 2 degrees of freedom, and the two degrees of freedom that were left from the vector, are gauged away. This can easily be seen by checking that the scalar, vector, and tensor parts transform as

$$\begin{aligned} \Phi &\rightarrow \Phi + \partial_0 \xi_0 \\ B &\rightarrow B - \xi_0 - \partial_0 f \\ \Psi &\rightarrow \Psi + \frac{1}{3} \nabla^2 f \\ F &\rightarrow F - 2f \\ S_i &\rightarrow S_i - \partial_0 f_i \\ T_i &\rightarrow T_i - f_i \\ t_{ij} &\rightarrow t_{ij}, \end{aligned} \quad (2.12)$$

which also shows a gauge invariant tensor. We are left with 6 degrees of freedom. These 6 degrees of freedom do not all describe gravitational waves. Further gauge fixing of the scalars and vectors is needed.

A convenient choice of gauge, which is commonly used to fix ξ , is the Lorentz gauge, $\partial_\mu \bar{h}^{\mu\nu} = 0$ [1]. Note that we are using the trace reversed metric here. The Lorentz gauge is always applicable, as we will show. Assume an arbitrary perturbation for which $\partial^\mu \bar{h}_{\mu\nu} \neq 0$. Then under an

infinitesimal coordinate transformation, this transforms as

$$\partial'^{\mu}\bar{h}'_{\mu\nu}(x') = \partial^{\mu}\bar{h}_{\mu\nu}(x) - \square\xi_{\nu}. \quad (2.13)$$

By simply choosing $\square\xi_{\nu} = \partial^{\mu}\bar{h}_{\mu\nu}$ the term on the left side will become zero, i.e., $\partial'^{\mu}\bar{h}'_{\mu\nu}(x') = 0$. A solution can always be found since the d'Alembertian operator is invertible. Hence, by choosing the appropriate ξ , the metric perturbation can always be written in the Lorentz gauge. Now that $\partial'^{\mu}\bar{h}'_{\mu\nu}(x') = 0$, we can of course continue making gauge transformations,

$$\partial''^{\mu}\bar{h}''_{\mu\nu}(x'') = \partial'^{\mu}\bar{h}'_{\mu\nu}(x') - \square\xi_{\nu} \quad (2.14)$$

$$= \partial^{\mu}\bar{h}_{\mu\nu}(x) - 2\square\xi_{\nu} \quad (2.15)$$

$$= -\partial^{\mu}\bar{h}_{\mu\nu}(x). \quad (2.16)$$

As one can see, to remain in the Lorentz gauge after this gauge transformation, the vector ξ needs to satisfy $\square\xi = 0$. Hence, the Lorentz gauge removes the 4 degrees of freedom discussed above; however, it leaves residual freedom for gauge transformations with $\square\xi = 0$. This is further fixed by the commonly used transverse traceless (TT) gauge, which is only valid in vacuum:

$$h_i^{iTT} = 0, \quad h_{0\mu}^{TT} = 0. \quad (2.17)$$

Note that in the TT gauge $\bar{h}_{\mu\nu}^{TT} = h_{\mu\nu}^{TT}$, and only the tensor t_{ij} with 2 degrees of freedom is left. These are the 2 degrees of freedom that describe the two polarizations of a gravitational wave. To summarize, the transverse traceless gauge and the Lorentz gauge combined to give the following constraints:

$$h_{0\mu}^{TT} = 0, \quad h_i^{iTT} = 0, \quad \partial^j h_{ij} = 0. \quad (2.18)$$

The linearized Einstein equations in terms of the trace-reversed metric now reduce to a simple expression:

$$\square h_{\mu\nu}^{TT} = \frac{-16\pi G}{c^4} \Lambda_{\mu\nu,\rho\sigma} T_{\rho\sigma}, \quad (2.19)$$

where the lambda tensor $\Lambda_{\mu\nu,\rho\sigma}$ is the TT projector which shall be discussed further in the second lecture.

2.4 Vacuum solutions

Let us think about a gravitational wave detector far away from any gravitational wave source. Hence, in a vacuum where $T_{\mu\nu} = 0$, such that

$$\square h_{\mu\nu}^{TT} = 0. \quad (2.20)$$

This has a plane wave solution,

$$h_{\mu\nu}^{TT}(x) = A_{\mu\nu}(k) \sin k^{\alpha} x_{\alpha}. \quad (2.21)$$

Due to the restrictions imposed by the TT gauge, we can conclude that the amplitude is traceless and purely spatial. What is left to ensure that we are in the *transverse* traceless gauge, is to check if the perturbation is transverse. In other words,

$$\partial^\mu h_{\mu\nu}^{TT} = k^\mu A_{\mu\nu}(k) \sin k^\alpha x_\alpha = 0. \quad (2.22)$$

This relation is true if the wavevector is orthogonal to the amplitude, $k^\mu A_{\mu\nu} = 0$. For example [1], if the wave is propagating in the \hat{z} -direction, then $A_{z\nu} = 0$. Considering that $A_{0\nu} = A_i^i = 0$ and $A_{\mu\nu}$ is also symmetric, we can generally write

$$\begin{aligned} A_{xx} &= -A_{yy} \equiv h_+, \\ A_{xy} &= A_{yx} \equiv h_x, \end{aligned} \quad (2.23)$$

and the rest is zero. Thus

$$A_{\mu\nu}(k) = \begin{pmatrix} 0 & 0 & 0 & 0 \\ 0 & h_+ & h_x & 0 \\ 0 & h_x & -h_+ & 0 \\ 0 & 0 & 0 & 0 \end{pmatrix}. \quad (2.24)$$

To check if this really is a solution let's plug it into the equation of motion

$$\square \bar{h}_{\mu\nu}^{TT} = k^\alpha k_\alpha A_{\mu\nu}(k) \sin k^\alpha x_\alpha = 0. \quad (2.25)$$

Note that not all components of $A_{\mu\nu}$ are zero, which means that

$$k^\alpha k_\alpha = 0 \rightarrow E^2 - P^2 = 0. \quad (2.26)$$

This is a rough proof that gravitational waves travel at the speed of light!

2.5 Effects of gravitational waves on test masses

To examine the effect of gravitational waves on mass, consider two test masses on a geodesic trajectory parametrized by $x^\mu(\tau)$ and $x^\mu(\tau) + \xi^\mu(\tau)$. The classical motion of a test particle at x^μ is obtained by extremizing the action. This gives the geodesic equation,

$$\frac{d^2 x^\mu}{d\tau^2} + \Gamma_{\rho\nu}^\mu(x) \frac{dx^\nu}{d\tau} \frac{dx^\rho}{d\tau} = 0 \quad (2.27)$$

while $x^\mu + \xi^\mu$ satisfies

$$\frac{d^2(x^\mu + \xi^\mu)}{d\tau^2} + \Gamma_{\rho\nu}^\mu(x + \xi) \frac{d(x^\nu + \xi^\nu)}{d\tau} \frac{d(x^\rho + \xi^\rho)}{d\tau} = 0. \quad (2.28)$$

It is assumed that ξ is much smaller than the length scale of the gravitational waves, such that we can expand to the first order in ξ . Then, taking the difference between the two geodesic equations will give the geodesic deviation equation,

$$\frac{d^2 \xi^\mu}{d\tau^2} + 2\Gamma_{\rho\nu}^\mu(x) \frac{dx^\nu}{d\tau} \frac{d\xi^\rho}{d\tau} + \xi^\sigma \partial_\sigma \Gamma_{\nu\rho}^\mu(x) \frac{dx^\nu}{d\tau} \frac{dx^\rho}{d\tau} = 0, \quad (2.29)$$

describing the motion of the test particles relative to each other. This can be rewritten in terms of the Riemann tensor,

$$\frac{d^2\xi^\mu}{d\tau^2} + R^\mu_{\nu\sigma\rho} \frac{dx^\rho}{d\tau} \frac{dx^\nu}{d\tau} \xi^\sigma.$$

We choose coordinates such that the Christoffel symbol vanishes at the spacetime position of the first test point particle. Assuming a non-relativistic motion of the test particles, thus $\frac{dx^i}{d\tau} \ll \frac{dx^0}{d\tau}$, and noticing from equation (2.4) that $R^i_{0j0} = \frac{-1}{2c^2} \ddot{h}^i{}^{TT}$, the geodesic deviation equation reduced to

$$\ddot{\xi}^i = -c^2 R^i_{0j0} \xi^j = \frac{1}{2} \ddot{h}^i{}^{TT} \xi^j. \quad (2.30)$$

As an example [1], let us consider the + polarisation and study the motion of test particles in the xy plane. In this case,

$$h_{ab}^{TT} = h_+ \sin \omega t \begin{pmatrix} 1 & 0 \\ 0 & -1 \end{pmatrix}, \quad a, b = \{x, y\}. \quad (2.31)$$

The distance between the particles can generally be written as

$$\xi_a(t) = (X_0 + \delta X(t), Y_0 + \delta Y(t)), \quad (2.32)$$

where (X_0, Y_0) are the unperturbed coordinates and $\delta X(t), \delta Y(t)$ are the displacements from the gravitational waves. Equation (2.30) results in

$$\delta \ddot{X} = \frac{-h_+}{2} (X_0 + \delta X) \omega^2 \sin \omega t, \quad (2.33)$$

$$\delta \ddot{Y} = \frac{h_+}{2} (Y_0 + \delta Y) \omega^2 \sin \omega t, \quad (2.34)$$

where the linear terms δX and δY on the right-hand side can be neglected, since $\delta X \ll X_0$ and $\delta Y \ll Y_0$. Integrating the equations and we get

$$\delta X = \frac{h_+}{2} X_0 \sin \omega t, \quad \delta Y = \frac{-h_+}{2} Y_0 \sin \omega t. \quad (2.35)$$

The result for a ring of test masses is shown in Fig. (2)

3 Lecture: Emission of gravitational waves

Having solved the linearized Einstein equation for the vacuum case in the last lecture, in the second lecture we focus on the Einstein equation with a source term, i.e.,

$$\square \bar{h}_{\mu\nu} = -\frac{16\pi G}{c^4} T_{\mu\nu}. \quad (3.1)$$

After having solved the above equation, we will discuss gravitational waves in a curved background and derive the energy-momentum tensor for gravitational waves. We close this lecture by deriving Einstein's quadrupole formula.

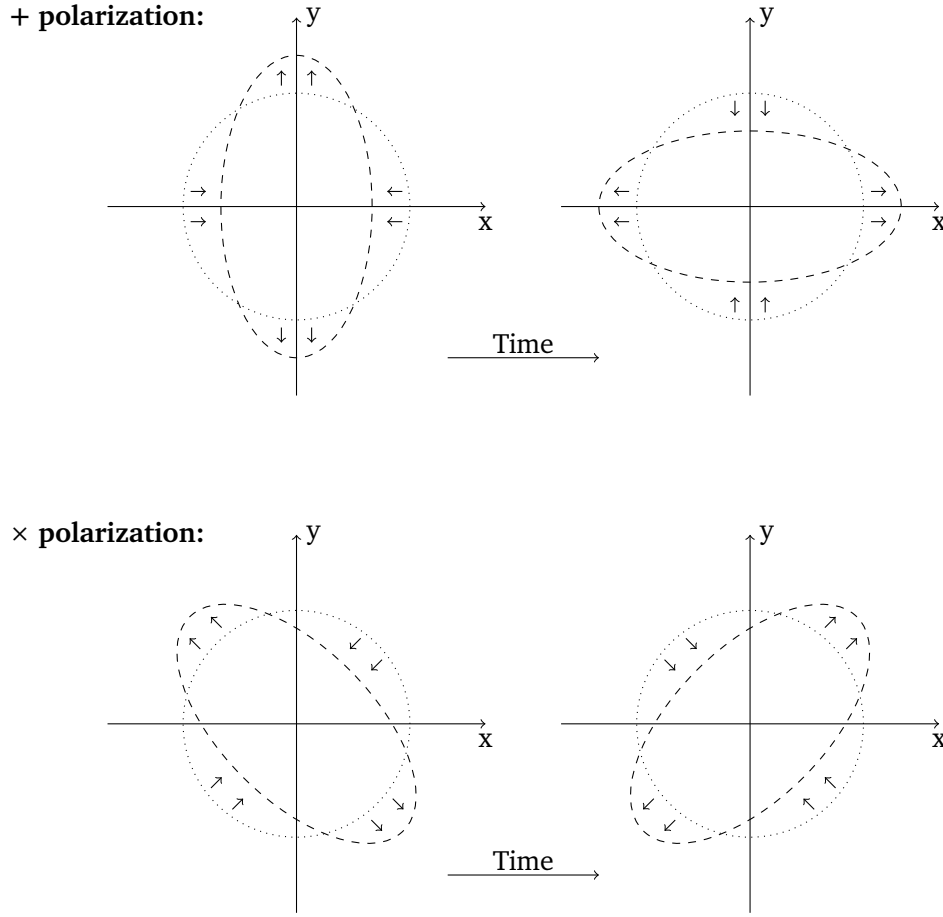


Figure 2: A gravitational wave traveling in z -direction with a $+$ polarization will curve spacetime such that a ring of test masses (gray dots) is alternating between a vertical and horizon elliptical shape, creating a $+$ sign. A \times polarized gravitational wave creates \times sign as shown in the bottom figure.

3.1 Gravitational waves emitted by source

Equation (3.1) is solved by using the Green function for the d'Alembertian operator \square ,

$$\square_x G(x^\sigma - y^\sigma) = \delta^{(4)}(x^\sigma - y^\sigma), \quad (3.2)$$

where x^σ and y^σ are depicted in Fig. 3. This is exactly how it is done in the analogous electromagnetic problem. The general solution is

$$\bar{h}_{\mu\nu}(x^\sigma) = -\frac{16\pi G}{c^4} \int G(x^\sigma - y^\sigma) T_{\mu\nu}(y^0, \vec{y}) d^4 y, \quad (3.3)$$

with $G(x^\sigma - y^\sigma) = -\frac{1}{4\pi|\vec{x}-\vec{y}|} \delta[|\vec{x}-\vec{y}| - (x^0 - y^0)] \theta(x^0 - y^0)$, and the theta function equals one when $x^0 > y^0$ [2]. After integrating over y^0 we obtain

$$\bar{h}_{\mu\nu}(t, \vec{x}) = \frac{4G}{c^4} \int \frac{1}{|\vec{x}-\vec{y}|} T_{\mu\nu}(t - |\vec{x}-\vec{y}|) d^3 y, \quad (3.4)$$

where $t = x^0$ and $t - |\vec{x} - \vec{y}| = t_r$ is referred to as the retarded time.

In the following, we will make the assumption that the source is far away and slowly moving. Hence the source is centered at a distance \vec{x} , and the edge of the source is at a distance $\vec{r} = \vec{x} - \vec{y}$, as is shown in Fig. 3. In terms of r , the gravitational wave takes the form

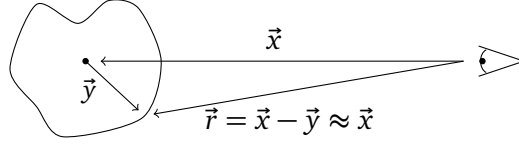


Figure 3: An observer observes the center of a gravitational wave source at a distance \vec{x} . The outer edge of the source is at a distance \vec{y} from the center and thus observed at a distance $\vec{r} = \vec{x} - \vec{y}$. The source is a large distance from the observer, hence $\vec{r} \approx \vec{x}$.

$$\bar{h}_{\mu\nu}(t, \vec{x}) = \frac{4G}{rc^4} \int d^3y T_{\mu\nu}(t - \frac{r}{c}, y). \quad (3.5)$$

As we have seen before, in the vacuum case, the temporal components are set to zero, and thus we are only interested in the spatial components. This is given by

$$\int d^3y T_{ij} = \frac{1}{2} \partial_0^2 \int d^3y y_i y_j T_{00}(y). \quad (3.6)$$

To prove this relation, note that the energy/momentum conservation implies $\partial_\mu T^{\mu\nu} = 0$, and thus we can derive

$$\begin{aligned} \partial_\mu T^{0\mu} &= \partial_0 T^{00} + \partial_k T^{0k} = 0 \\ \partial_0^2 T^{00} &= -\partial_k \partial_0 T^{0k} = \partial_k \partial_l T^{lk} \\ y_i y_j \partial_0^2 T^{00} &= y_i y_j \partial_k \partial_l T^{lk} = 2T^{ij} \end{aligned} \quad (3.7)$$

In the second line, energy/momentum conservation was used again and the last step is obtained by partial integration and $\partial_k y_i = \delta_{ki}$. Thus

$$\bar{h}_{ij}(t, \vec{x}) = \frac{2G}{c^4} \frac{1}{r} \partial_0^2 \int d^3y y_i y_j T_{00}(t - \frac{r}{c}, y), \quad (3.8)$$

where it is conventional to define the integral as the tensor moment of the source $I_{ij}(t - \frac{r}{c})$. The resulting formula

$$\bar{h}_{ij}(t, \vec{x}) = \frac{2G}{c^4} \frac{1}{r} \partial_0^2 I_{ij}(t - \frac{r}{c}) \quad (3.9)$$

is known as the quadrupole formula.

The transverse traceless gauge for gravitational waves outside the sources and propagating in \hat{n} direction is found by projecting the solution onto the TT gauge [1]. For this, we introduce a transverse projector $P_{ij} = \delta_{ij} - n_i n_j$, with $\hat{n} = \frac{\vec{k}}{k}$, which is used to construct the Lambda tensor $\Lambda_{ij,kl} \equiv P_{ik} P_{jl} - \frac{1}{2} P_{ij} P_{kl}$. The Lambda tensor $\Lambda_{ij,kl}$ is transverse in *all* indices, i.e., $n^i \Lambda_{ij,kl} = 0$, and

it projects out the trace $\Lambda_{ii,kl} = \Lambda_{ij,kk} = 0$. By projecting the metric perturbation, we obtain the traceless transverse version

$$h_{ij}^{TT} = \Lambda_{ij,kl} h_{kl}. \quad (3.10)$$

As an example, for a wave in \hat{z} direction, the projector will have the form

$$P = \begin{pmatrix} 1 & 0 & 0 \\ 0 & 1 & 0 \\ 0 & 0 & 0 \end{pmatrix}, \quad (3.11)$$

and any arbitrary symmetric matrix will take the form

$$\Lambda_{ij,kl} \underbrace{A_{kl}}_{\substack{\text{Arbitrary sym-} \\ \text{metric } 3 \times 3 \\ \text{matrix}}} = \begin{pmatrix} \frac{1}{2}(A_{11} - A_{22}) & A_{12} & 0 \\ A_{21} & -\frac{1}{2}(A_{11} - A_{22}) & 0 \\ 0 & 0 & 0 \end{pmatrix}. \quad \begin{matrix} \curvearrowright h_x \\ \curvearrowright h_+ \end{matrix}$$

To summarize, in the TT gauge, the metric perturbation is given by the quadrupole formula which takes the form

$$h_{ij}^{TT}(t, \vec{x}) = \frac{2G}{c^4} \frac{1}{r} \Lambda_{ij,kl} \ddot{I}_{kl}(t - \frac{r}{c}), \quad (3.12)$$

where the quadrupole moment is defined as

$$\mathbb{I} \equiv \int d^3y (y_k y_l - \frac{1}{3} y^2 \delta_{kl}) T_{00} = I_{kl} - \frac{1}{3} I_m^m \delta_{kl}. \quad (3.13)$$

This is the trace-free version of I . It is a bit redundant with the projector Λ , although often useful in practice!

3.2 Energy momentum tensor of gravitational waves

So far, we have considered linearized Einstein equations as an expansion around the flat spacetime metric $\eta_{\mu\nu}$. The fluctuations around the static flat background are the gravitational waves. In a general dynamical curved spacetime with a metric

$$g_{\mu\nu}(x) = \bar{g}_{\mu\nu}(x) + h_{\mu\nu}(x), \quad (3.14)$$

the question arises whether the curvature is actually a gravitational wave or part of the background [1]. In the latter case, the gravitational wave can locally be gauged away. How do we decide which part is the background and which part is a gravitational wave? A natural splitting arises when picking the right scale. Denoting the length of the background by L_b , and the wavelength of the gravitational wave by λ_{GW} ⁶. A suitable length scale d is large enough to observe λ_{GW} and

⁶Note that the typical length scale for the gravitational wave is $\lambda_{GW} = \frac{\lambda}{2\pi}$ instead of λ and is also known as the reduced wavelength.

small enough such that the background is approximately flat. This method of separation of the metric into a smooth background and perturbations is called short-wave expansion.

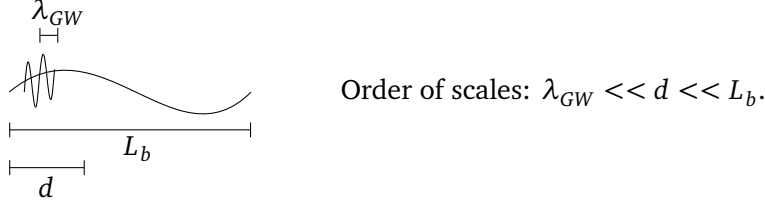


Figure 4: A visualization of short-wave expansion. The spacetime is separated in a background with a length L_b , and a gravitational wave with wavelength λ_{GW} . This separation arises natural when considering a scale length d , such that $\lambda_{GW} \ll d \ll L_b$.

How does this perturbation propagate in the background spacetime and how does it affect the background metric [1]? To address these questions we expand the Einstein equations around a background metric. In this expansion there are typically two small parameters, the amplitude h and $\frac{\lambda_{GW}}{L_b}$ (or $\frac{f_B}{f}$). So let us expand $G_{\mu\nu}$ in powers of h :

$$G_{\mu\nu} = G_{\mu\nu}^{(B)} + G_{\mu\nu}^{(1)} + G_{\mu\nu}^{(2)} + \dots \quad (3.15)$$

The term $G^{(B)}$ is related to the background and solely constructed from $\bar{g}_{\mu\nu}$. $G_{\mu\nu}^{(1)}$ is linear in $h_{\mu\nu}$ and contains only high-frequency modes, while $G_{\mu\nu}^{(2)}$ is quadratic and contains *both* high and low frequencies. For instance, consider a quadratic term $h_{\mu\nu}h_{\rho\sigma}$, where $h_{\mu\nu}$ and $h_{\rho\sigma}$ contain a mode with wave-vector \vec{k}_1 and \vec{k}_2 , respectively, with $|\vec{k}_1|, |\vec{k}_2| \gg \frac{1}{d}$. The high wave vectors can combine such that the sum becomes a low wave vector mode, $|\vec{k}_1 + \vec{k}_2| \ll \frac{1}{d}$. In this manner, the Einstein equations can be split into equations for high frequencies and for low frequencies. We will focus on the small \vec{k} ⁷ part of Einstein's equation

$$\begin{aligned} G_{\mu\nu}^B &= -[G_{\mu\nu}^{(2)}]^{small \vec{k}} + \frac{8\pi G}{c^4}[T_{\mu\nu}]^{small \vec{k}} \\ &= -\langle G_{\mu\nu}^{(2)} \rangle_d + \frac{8\pi G}{c^4}[T_{\mu\nu}]_d \end{aligned} \quad (3.16)$$

In the second line, we average over a spatial volume at a scale d . This does not affect the modes with a wavelength of order L_B , since these are more or less constant over a distance d . On the other hand, the fast oscillating waves of order λ_{GW} will average zero. The attentive observer will notice that the above technique is basically a renormalization group transformation. We take the fundamental equations of the theory and “integrate out” the small (high energy) fluctuations, to obtain an effective theory that describes physics at the length scale L_B . The result is the “course-grained” Einstein equations.

An explicit computation of $G_{\mu\nu}$ to 2nd order in the TT gauge will give

$$R_{\mu\nu}^{(2)} = \dots = \frac{1}{4} \partial_\mu h_{\alpha\beta} \partial_\nu h^{\alpha\beta} + 12 \text{ terms}, \quad (3.17)$$

⁷ $\vec{k} = \frac{2\pi}{\lambda} = \frac{1}{\lambda_{GW}}$

$$\langle R_{\mu\nu}^{(2)} \rangle_d = -\frac{1}{4} \langle \partial_\mu h_{\alpha\beta}^{TT} \partial_\nu h^{TT\alpha\beta} \rangle, \quad \langle R^{(2)} \rangle = 0, \quad \langle R^{(1)} \rangle = 0. \quad (3.18)$$

The averaged 2nd order $G_{\mu\nu}$ is defined as the energy-momentum tensor of gravitational waves. Gravitational waves carry energy that curves the background, because of the way it enters in (3.16).

$$t_{\mu\nu} = -\langle G_{\mu\nu}^{(2)} \rangle_d = -\frac{c^4}{8\pi G} \left\langle R_{\mu\nu}^{(2)} - \frac{1}{2} \bar{g}_{\mu\nu} R^{(2)} \right\rangle \quad (3.19)$$

The explicit expression for $t_{\mu\nu}$ is found by substituting $R_{\mu\nu}^{(2)}$ into equation (3.19).

$$t_{\mu\nu} = \frac{c^4}{32\pi G} \langle \partial_\mu h_{\alpha\beta}^{TT} \partial_\nu h^{\alpha\beta TT} \rangle. \quad (3.20)$$

Furthermore, the energy density of gravitational waves, defined as the 00 - component of the energy stress tensor, is found to be

$$\rho_{GW} = t_{00} = \frac{c^4}{32\pi G} \langle \dot{h}_{ij}^{TT} \dot{h}^{ijTT} \rangle. \quad (3.21)$$

3.3 Einstein's quadrupole formula

Given the energy density of gravitational waves, the energy of the gravitational radiation in a volume V is given by

$$E_{GW} = \int_V d^3x t^{00}. \quad (3.22)$$

Demanding conservation of energy-momentum tensor, $\partial_\mu t^{\mu\nu} = 0$, implies that

$$\int_V d^3x (\partial_0 t^{00} + \partial_i t^{i0}) = 0 \quad (3.23)$$

and we can write

$$\frac{dE_{GW}}{c dt} = - \int_V d^3x \partial_i t^{0i} = - \int_S dA n_i t^{0i}, \quad (3.24)$$

where n_i is the outer normal to the surface and dA the surface element of the volume V . Now, let S be a spherical surface at a large distance r from the source. For a spherical volume, the surface element is $dA = r^2 d\Omega$, and its normal is $\hat{n} = \hat{r}$. Then

$$\frac{dE_{GW}}{dt} = -\frac{r^2}{c} \int d\Omega t^{0r} = \frac{r^2}{c} \int d\Omega t^{00}. \quad (3.25)$$

Hence, we have

$$P_{GW} = \frac{dE_{GW}}{dt} = \frac{r^2 c^3}{32\pi G} \int d\Omega \langle \dot{h}_{ij}^{TT} \dot{h}_{ij}^{TT} \rangle = \frac{G}{8\pi c^5} \int d\Omega \Lambda_{ij,kl}(\hat{n}) \langle \ddot{I}_{ij} \ddot{I}_{ij} \rangle, \quad (3.26)$$

which is known as Einstein's quadrupole formula:

$$P_{GW} = \frac{G}{5c^5} \langle \ddot{I}_{ij} \ddot{I}_{ij} \rangle, \quad (3.27)$$

describing the power emitted by a source with tensor moment I_{ij} . This allows for example to compute the gravitational wave emitted by a black hole binary.

4 Lecture: The stochastic gravitational wave background

In the last lectures, we generically described gravitational waves, identifying the two propagating degrees of freedom from general relativity. Now, we specialize our studies on the topic of stochastic gravitational waves, by deriving the main properties, and then describing current searches.

4.1 The gravitational wave background

Stochastic gravitational wave backgrounds (SGWBs) are defined as the superposition of gravitational waves with different wave numbers \mathbf{k} (both in magnitude and direction). They can have astrophysical or cosmological origins and typically are isotropic, unpolarized, and gaussian⁸. It is then very similar to the cosmic microwave background (CMB) from the electromagnetic spectrum. SGWBs can allow us to reach stages where CMB cannot guide us since gravitational waves can travel freely through the hot plasma of the early universe, which is not transparent to photons.

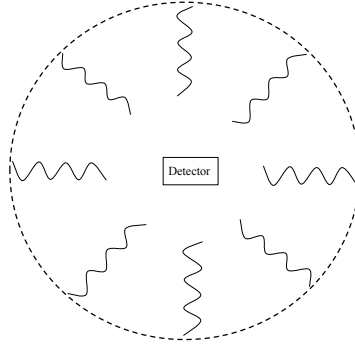


Figure 5: Here we show a schematic representation of the propagation and detection of SGWBs. The circle represents some cosmic event (gravitational wave source). The waves then propagate through the universe. Occasionally they find a detector. The signal from SGWBs act as additional "noise" in a gravitational wave detector.

Possible early-universe sources emitted gravitational waves in the past. These signals are continuously reaching us, coming from all directions. The gravitational wave spectral shape is given by

$$\Omega_{GW} = \frac{1}{\rho_c} \frac{d\rho_{GW}}{d \ln k}. \quad (4.1)$$

Signals from SGWBs are small and it is challenging to detect them because what arrives in the detector is similar to a noise source. Therefore, they can serve as a cosmological history book, which is tricky to decipher. Phenomena like inflation, primordial black holes, cosmic strings, and phase transitions are possible cosmic sources. These primordial sources are relevant for beyond-Standard-Model theories. These theories usually rely on energy scales far beyond what Earth-based experiments can achieve but were reached during the high-temperature stages of the early universe⁹.

⁸From astrophysical sources, this follows from the central limit theorem. For cosmological sources, this statement is model-dependent.

⁹For instance, current accelerators reach center-of-mass energies of the order $\sim 10^4$ GeV, which is enough to probe the electroweak phase transition scale, ~ 100 GeV, but it is far beyond grand-unification scales of order $\sim 10^{16}$ GeV.

So far, pulsar time array (PTA) collaborations - have claimed statistical evidence for excess noise that early-universe gravitational waves could potentially explain, see, for instance, the reviews [4–6]. Beyond PTAs, gravitational-wave detectors will reach the frequency region required for SGWBs, with LISA [7] and the 3rd generation of ground-based detectors [8]. Notice that SGWB signals are different than those LIGO-Virgo detected (transient signals) in the recent gravitational wave observation from binary mergers [9, 10].

4.2 gravitational waves in expanding FRW universe

Setting $c = 1$, the metric of an expanding FRW universe is given by

$$ds^2 = -dt^2 + a(t)^2 dx^i dx_i = -a(\tau)^2 (d\tau^2 - g_{ij} dx^i dx^j), \quad (4.2)$$

where τ is the conformal time and a the scale factor. Expanding around a flat homogeneous cosmological background $g_{ij} = \delta_{ij} + h_{ij}$, the linearized field equations are

$$\square \bar{h}_{ij}(\mathbf{x}, \tau) - \frac{2a'}{a} \bar{h}'_{ij}(\mathbf{x}, \tau) = -16\pi G T_{ij}, \quad (4.3)$$

where derivatives with respect to conformal time are denoted by primes. Notice that the second term on the left-hand side vanishes for a static universe, and we recover the usual linearized Einstein gravitational wave equation (see the first lecture). By Fourier transforming and defining $\tilde{h}_\lambda \equiv a h_\lambda$, where $\lambda = +, \times$ are the two polarization modes of the gravitational wave, we can rewrite the field equations as

$$\tilde{h}_\lambda''(\mathbf{k}, \tau) + \left(k^2 - \frac{a''}{a} \right) \tilde{h}_\lambda(\mathbf{k}, \tau) = 16\pi G a T_\lambda(\mathbf{k}, \tau). \quad (4.4)$$

We can approximate in the following two cases: $k^2 \gg (aH)^2$ (sub-horizon) and $k^2 \ll (aH)^2$ (super-horizon). In vacuum, for the **sub-horizon** case, (4.4) reduces to

$$\tilde{h}_\lambda''(\mathbf{k}, \tau) + k^2 \tilde{h}_\lambda(\mathbf{k}, \tau) \approx 0, \quad (4.5)$$

whose solution for \tilde{h} is oscillatory. Consequently,

$$h_\lambda(\mathbf{k}, \tau) \approx \frac{A_\lambda}{a} \cos(k\tau + \varphi), \quad (4.6)$$

where $A_\lambda = A_\lambda(\mathbf{k})$ is a constant in time. Notice that wave amplitude decays as the universe expands! For the **super-horizon** case, we have instead

$$2a'h'_\lambda + ah''_\lambda \approx 0, \quad (4.7)$$

whose solution is

$$h_\lambda = A_\lambda + B_\lambda \int_0^\tau \frac{d\gamma}{a(\gamma)^2} \approx \text{constant}, \quad (4.8)$$

where $A_\lambda = A_\lambda(\mathbf{k})$ and $B_\lambda = B_\lambda(\mathbf{k})$ are constant in time. Here we have used the fact that the integral decays in the expanding universe's history. Thus, gravitational waves are “frozen” outside the Hubble horizon. This mechanism is the same one occurring in inflation. After re-entry in the horizon, tensor perturbations become sub-horizon modes again, as described by (4.6). Let us focus on these sub-horizon modes.

A useful parametrization for the sub-horizon modes is [11]

$$h_{ij}^{TT}(\mathbf{x}, \tau) = \sum_{\lambda=+, \times} \int \frac{d^3k}{(2\pi)^3} h_\lambda(\mathbf{k}) \mathcal{T}_k(\tau) e_{ij}^\lambda(\hat{k}) e^{-i(k\tau - \mathbf{k}\cdot\mathbf{x})}. \quad (4.9)$$

For this parametrization, we define an initial time τ_* as the time of formation or horizon entry, or for sub-horizon sources, as the time of gravitational wave emission, i.e. when the decaying behavior ($1/a$) starts; h_λ is the Fourier coefficient at time $\tau = \tau_*$; $\mathcal{T}_k(\tau)$ is the transfer function given here by the ratio $a(\tau_*)/a(\tau)$ (notice we have factored out $1/a$); and e_{ij}^λ are the components of the polarization tensor that maps the Cartesian coordinates of the tensor h_{ij}^{TT} to its $+, \times$ degrees of freedom, as defined in the previous lecture.

We will use the equation for the energy density associated with gravitational waves in Sec. 3,

$$\rho_{GW}(\tau) = \frac{1}{32\pi G} \langle \dot{h}_{ij}^{TT}(\mathbf{x}, t) \dot{h}^{TTij}(\mathbf{x}, t)^* \rangle. \quad (4.10)$$

Since we are using conformal time, $\dot{h}_{ij} = (1/a)h'_{ij}$, $\mathcal{T}'_k = -\mathcal{T}_k(a'/a)$ and $\mathcal{H} = a'/a$, for $a = a(\tau)$. Therefore,

$$\dot{h}_{ij}^{TT}(\mathbf{x}, t) = -\frac{1}{a} \sum_\lambda \int \frac{d^3k}{(2\pi)^3} h_\lambda(\mathbf{k}) \mathcal{T}_k(\tau) e_{ij}^\lambda(\hat{k}) (ik + \mathcal{H}) e^{-i(k\tau - \mathbf{k}\cdot\mathbf{x})}, \quad (4.11)$$

and

$$\begin{aligned} \rho_{GW}(\tau) = \frac{1}{32\pi G} \frac{1}{a^2} \sum_{\lambda_1 \lambda_2} \int \frac{d^3k_1}{(2\pi)^3} \int \frac{d^3k_2}{(2\pi)^3} \langle h_\lambda(\mathbf{k}_1) h_{\lambda'}(\mathbf{k}_2) \rangle e_{ij}^\lambda(\hat{k}_1) e_{ij}^{\lambda'}(\hat{k}_2) \mathcal{T}_{k_1} \mathcal{T}_{k_2} \times \\ \times (ik_1 + \mathcal{H})(-ik_2 + \mathcal{H}) e^{-i(k_1 - k_2)\tau} e^{-i(\mathbf{k}_2 - \mathbf{k}_1)\cdot\mathbf{x}} \end{aligned} \quad (4.12)$$

The last term simplifies after assuming homogeneity and isotropy since the following expression holds

$$\langle h_\lambda(\mathbf{k}_1) h_{\lambda'}(\mathbf{k}_2) \rangle = (2\pi)^3 \delta_{\lambda\lambda'} \delta^3(\mathbf{k}_1 - \mathbf{k}_2) P_\lambda(|\mathbf{k}_1|), \quad (4.13)$$

where $P(k)$ is the non-normalized tensor power spectrum. We can write the energy density associated with SGWBs as

$$\rho_{GW}(\tau) = \frac{1}{32\pi G} \frac{1}{a^2} \sum_\lambda \int \frac{d^3k}{(2\pi)^3} \mathcal{T}_k^2 |ik + \mathcal{H}|^2 e_{ij}^\lambda e_{ij}^\lambda(k) P_\lambda(k). \quad (4.14)$$

For each polarization mode, $e_{ij}^\lambda e_{ij}^\lambda = 1$, since $e_{ij}^{\lambda_1} e_{ij}^{\lambda_2} = \delta_{\lambda_1, \lambda_2}$. Since we are working with **sub-horizon modes** and $|ik + \mathcal{H}|^2 = k^2 + \mathcal{H}^2 = k^2 + (aH)^2$, we can approximate $aH \ll k$ so that

$$\rho_{GW}(\tau) = \frac{1}{32\pi G} \frac{1}{a^2} \sum_\lambda \int \frac{d^3k}{(2\pi)^3} \mathcal{T}_k(\tau)^2 k^2 P_\lambda(k). \quad (4.15)$$

Hence, at a time τ_0 :

$$\rho_{GW}(\tau_0) = \frac{1}{32\pi G} \frac{1}{a^2(\tau_0)} \frac{4\pi}{(2\pi)^3} \int (k^2 dk) \times k^2 \sum_\lambda P_\lambda(k) \frac{a^2(\tau_*)}{a^2(\tau_0)}. \quad (4.16)$$

The term $\sum_\lambda P_\lambda(k)$ can be identified with the primordial power spectrum, and $\frac{a^2(\tau_*)}{a^2(\tau_0)}$ tells the cosmological history. We can also relate the energy density ρ_{GW} to the gravitational wave spectral shape Ω_{GW} through (4.1),

$$\rho_{GW} = \rho_c \int d(\log k) \frac{1}{\rho_c} \frac{\partial \rho_{GW}}{\partial \log k} = \rho_c \int d(\log k) \Omega_{GW}(k, \tau_0), \quad (4.17)$$

so that we can obtain the gravitational wave spectrum $\Omega_{GW}(k, \tau_0)$ by comparing the last expression with (4.16). The critical energy density is given by $\rho_c = (3H_0^2)(8\pi G)$. Therefore,

$$\Omega_{GW}(k, \tau_0) = \frac{k^5}{24\pi^2 H_0^2} \sum_\lambda P_\lambda(k) \frac{a^2(\tau_*)}{a^4(\tau_0)}. \quad (4.18)$$

Why is Ω_{k, τ_0} relevant? Because it is the spectrum of gravitational wave density, carrying information on the source and cosmic history as measured today.

By defining the power spectra of tensor fluctuations as

$$\Delta_t^2 = \frac{k^3}{2\pi^2} \sum_\lambda P_\lambda(k) \quad (4.19)$$

we can rewrite

$$\Omega_{GW}^0(k) = \frac{\Delta_t^2 k^2 a^2(\tau_*)}{12 H_0^2 a^4(\tau_0)} = \frac{\Delta_t^2}{12} \left(\frac{k}{a_* H_*} \right)^2 \frac{a_*^4 H_*^2}{a_0^4 H_0^2}, \quad (4.20)$$

where $a_* = a(\tau_*)$, $H_* = H(\tau_*)$ and the index 0 denotes quantities at today's time writing.

Take, for instance, the case of *single field slow-roll inflation*¹⁰, for τ_* in radiation domination. The power spectrum for each polarization mode is

$$P_\lambda(k) = \left(\frac{2}{M_p} \right)^2 \left(\frac{H_{\text{inflation}}^2}{2k^3} \right), \quad (4.21)$$

where $M_p = 1/(8\pi G)$. We will deduce this expression later, see Eq. (6.15). It follows that Δ_t^2 is constant, given by¹¹

$$\Delta_t^2 = 2H_{\text{inflation}}^2 / (\pi^2 M_p^2). \quad (4.22)$$

At the time of horizon entry, $a_* H_* = k$. So, Ω_{GW}^0 does not depend on k , and the gravitational wave spectrum and the energy density decrease with a^4 , as expected for radiation.

We can also plot the expected shape of such gravitational wave spectrum as a function of the observed frequency, see Fig. 6. If a gravitational wave is emitted with some frequency f_* at time τ_* and assuming horizon sized source, then the observed frequency at time τ_0 is red-shifted, given by (see more in Sec. 5.1)

$$f_0 = f_* \frac{a(\tau_*)}{a(\tau_0)} \sim H_* a_*. \quad (4.23)$$

¹⁰During inflation, gravitational waves are created from quantum fluctuations in quasi-de-Sitter spaces. Here we assume that the polarization modes are the same, i.e., $P_+ = P_-$, which is a valid assumption for single-field slow-roll inflation, that shows no preference for either polarization, and the SGWB is unpolarized.

¹¹In the inflationary period, $a(t) = e^{\Lambda t}$, for constant $\Lambda = H_{\text{inflation}}$. Since the k^3 from the power spectrum cancels the corresponding term in the definition of the tensor fluctuation, Δ_t^2 is constant for any value of k .

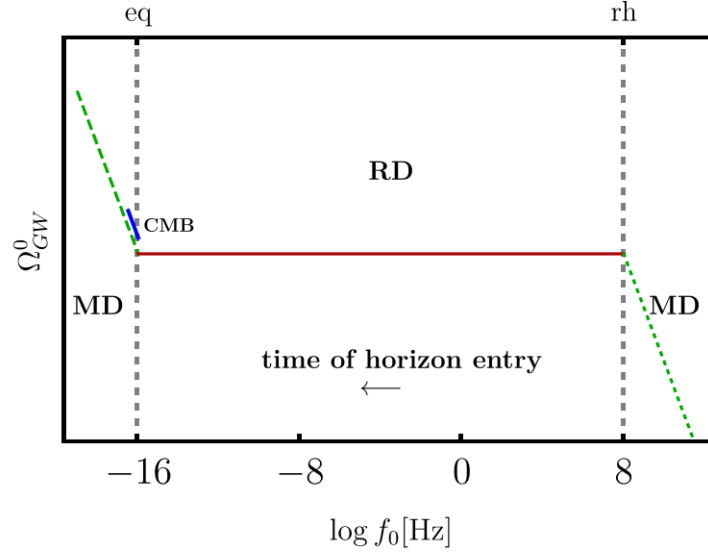


Figure 6: Plot in logarithm scale of the gravitational wave power spectrum from single field slow-roll inflation versus frequency (observed today), in Hz. Notice that time flows in the opposite direction of the frequency axis since $f_0 \sim a_*^{-1}$. The spectrum does not depend on the frequency during the radiation-domination era (RD, red, solid line, $\omega_* = 1/3$). During the matter-domination era (MD, green, dashed line, $\omega_* = 0$), $\Omega_{GW}^0 \sim f_0^{-2}$. The acronym “eq” stands for matter-radiation equality, and “rh” for reheating (the last stage of inflation, which takes into account all processes from the decay of the inflaton field in order to establish the hot thermal bath of the Big Bang). We assumed that reheating (MD, green, dotted line) occurred at $f_0 \sim 10^8 \text{ Hz}$. During reheating $\omega_* = \langle \omega \rangle = 0$, as MD. On left, we also show the power spectrum of CMB (blue, thick line, $r = \Delta_t^2/\Delta_s^2 < 0.1$), related to tensor anisotropies on the last scattering surface, during the matter-domination era.

Therefore $\Omega_{GW}^0 \sim f_0^2 a_*^2$. As $H_*^2 \sim \rho$ and during radiation domination $\rho \sim a^{-4}$, then $H_* \sim a^{-2}$, $f_0 \sim a_*^{-1}$, and finally $\Omega_{GW}^0 \sim (f_0)^0$, i.e., the gravitational wave spectrum does not depend on the observed frequency. Instead, if the gravitational wave was emitted during a matter-dominated era, then $H_* \sim a^{-3/2}$, $f_0 \sim a_*^{-1/2}$, and finally $\Omega_{GW}^0 \sim f_0^{-2}$. This is the behavior expected for inflationary gravitational waves. Different primordial sources will depend on f_0 in different ways. See Sec. 5.

Notice also that we did not take into account any changes in the number of relativistic (g_*) and entropy ($g_{*,s}$) degrees of freedom. In general, by considering the evolution of the universe and taking care of the Standard Model degrees of freedom, we can assume that the gravitational wave density decays like radiation so that the gravitational wave density spectrum can be expressed as a function of $\Omega_{rad}^0 \sim 10^{-5}$ (which accounts for radiation) and the degrees of freedom as

$$\Omega_{gw}^{\text{observed}}(k) = \frac{\Omega_{rad}^0}{24} \left(\frac{g_*(k)}{g_*^0} \right) \left(\frac{g_{*,s}^0}{g_{*,s}(k)} \right)^{4/3} \Omega_{gw}^{\text{emitted}}(k). \quad (4.24)$$

4.3 Searching for SGWBs

In this section, we describe how we can detect SGWBs by using Michelson interferometers. The experiment detects light signals only when gravitational waves disturb the perfect destructive

interference pattern.

4.3.1 Experimental setting

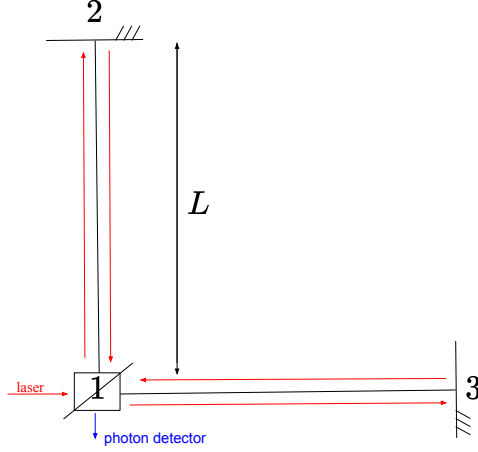


Figure 7: Michelson interferometer: the experiment consists in splitting laser light beams through a beam splitter at 1 in two different paths (here each arm has length L), reflecting them with two mirrors located at 2 and 3, and recombining them back in 1 so that interference patterns can be created (in particular, perfect destructive interference) in the photon detector (dark fringe).

According to the setting in Fig. 7, we need to compute the time delay associated with light departing and going back to 1. There are at least two possible frames: in the TT frame, gravitational waves change the photon propagation, and the “free-falling” mirrors do not move; in the proper detector frame, gravitational waves change the distance between the beam-splitter and mirrors.

Let us work in the TT frame. If light travels with $c = 1$, it takes L to travel from 1 to the mirror and $2L$ back to 1. In the $\hat{l} = \mathbf{x}$ direction, the time delay for a light signal emitted at time t is given by¹²:

$$\Delta T(t) = \frac{1}{2} \hat{l}^a \hat{l}^b \int_0^L h_{ab}(t+s, \mathbf{x} + s\hat{l}) ds, \quad a, b = 1, 2, 3; \quad (4.25)$$

where

$$h_{ab}(t, \mathbf{x}) = \int d^3k e^{-2\pi i \mathbf{k} \cdot \mathbf{x}} \sum_{\lambda} \hat{e}_{ab, \lambda}(\hat{k}) h_{\lambda}(t, \mathbf{k}). \quad (4.26)$$

The time delay, to be measured at time t , associated with the return trip is $\Delta T_{12}(t-2L) + \Delta T_{21}(t-L)$. We also expect to find some noise $n_1(t)$. Thus, we write

$$s_{12}(t) = \Delta T_{12}(t-2L) + \Delta T_{21}(t-L) + n_1(t) \quad (4.27)$$

$$= L \int \frac{d^3k}{(2\pi)^3} \sum_{\lambda} I_{\lambda}^{12}(\mathbf{k}) h_{\lambda}(t-L, \mathbf{k}) + n_1(t), \quad (4.28)$$

¹²Here, it suffices to use flat spacetime. There is no relevant back-reaction of the gravitational waves in the spacetime where they are propagating, according to (3).

where we have defined the single-arm detector response as

$$I_{\lambda}^{12}(\mathbf{k}) = \frac{1}{2} \hat{l}^a \hat{l}^b \hat{e}_{ab,\lambda}(\hat{k}) e^{-2\pi i \mathbf{k} \cdot \mathbf{x}} \times \left(e^{-\pi i k L (1 + \hat{k} \cdot \hat{l})} \frac{\sin(\pi k L (1 - \hat{k} \cdot \hat{l}))}{\pi k L (1 - \hat{k} \cdot \hat{l})} + e^{\pi i k L (1 - \hat{k} \cdot \hat{l})} \frac{\sin(\pi k L (1 + \hat{k} \cdot \hat{l}))}{\pi k L (1 + \hat{k} \cdot \hat{l})} \right). \quad (4.29)$$

Notice that this expression tells us the direction in the detector is more sensitive! It also tells us something about frequency modes: the terms in the last bracket tend to 2 for $kL \ll 1$ (small frequency modes) and to 0 for $kL \gg 1$ (large frequency modes). For example, LIGO works within the low-frequency limit.

From the response function, there is suppression for both small and large frequency modes. For the large ones, the signal drops as $(\sin x)/x$ for $k \gg 1/L$. For the small ones, the response function is constant for $k \ll 1/L$. As the noise grows at low frequencies, sensitivity is lost.

4.3.2 Overlap reduction function

Assuming isotropic SGWB, the measured time delay s_{α} can be averaged

$$\langle s_{\alpha}^2 \rangle = L^2 \int \frac{d^3 k}{(2\pi)^3} \sum_{\lambda} P_{\lambda}(k) |I_{\lambda}^{12} - I_{\lambda}^{13}|^2 + \langle n^2 \rangle, \quad (4.30)$$

where P_{λ} is the power spectrum introduced in (4.13), $I_{\lambda}^{\alpha} = I_{\lambda}^{12} - I_{\lambda}^{13}$ and $\langle n^2 \rangle$ is the instrumental noise from different possible sources. P_{λ} depends on the gravitational wave signal and I_{λ}^{α} on the detector response.

In such cases, the main obstacle is noise. Consider that noise severely affects the data for very tiny time delays (which we expect from stochastic gravitational waves). Now, assume that there are two interferometers α and β , as shown in Fig. 8. Then,

$$\langle s_{\alpha} s_{\beta} \rangle = L^2 \int \frac{d^3 k}{(2\pi)^3} \sum_{\lambda} P_{\lambda}(k) I_{\lambda}^{\alpha*}(\mathbf{k}, \mathbf{x}_1) I_{\lambda}^{\beta}(\mathbf{k}, \mathbf{x}_2), \quad (4.31)$$

i.e., there is cross-correlation. Ideally, the two detectors are far away so that their instrumental noises are not correlated $\langle n_{\alpha} n_{\beta} \rangle = 0$. The signal is reduced by *overlap reduction function*¹³, which is essential for the detection of stochastic signals.

4.3.3 Monopole response function

Let us consider isotropic, unpolarized SGWB. For this case, we can define the monopole response function as

$$\mathcal{M}(k) = \sum_{\lambda} \int d\Omega |I_{\lambda}^{\alpha}|^2. \quad (4.32)$$

¹³Although we get rid of the noise by considering two detectors, the measured time delay now depends on the distance between them, see Fig. 8. The overlap reduction function, therefore, depends on the response of the individual detectors as well as their relative geometry. For pulsar time arrays, the overlap reduction function is known as the *Hellings-Downs curve* [12].

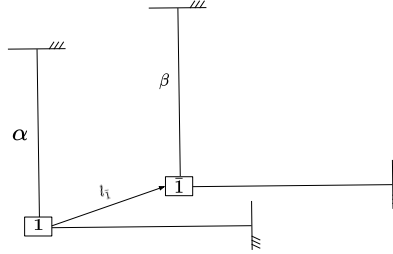


Figure 8: Two Michelson interferometers. We put the origin of the coordinate system at 1. To describe the location of the second detector, we need to include the vector from 1 to $\bar{1}$, where $\bar{1}$ is the central point of the second detector. Therefore, $\langle s_{\alpha s_{\beta}} \rangle$ depends on the distance between the interferometers.

By using the power spectra of tensor fluctuations given by (4.19), we can express the averaged time delay as

$$\frac{\langle s_{\alpha}^2 \rangle}{L^2} = \frac{1}{8\pi} \int d(\ln k) \Delta_t^2 \left(\sum_{\lambda} \int d\Omega |I_{\lambda}^{\alpha}|^2 \right) \equiv \frac{1}{8\pi} \int d(\ln k) \Delta_t^2 \mathcal{M}(k). \quad (4.33)$$

The dependence on the signal is due to Δ_t^2 . The dependence on the configuration of the detector is due to $\mathcal{M}(k)$. Then, by measuring the time delay and knowing the configuration of the detector, it is possible to get the signal!

Take, for instance, the case of LIGO, whose two detector arms are oriented perpendicularly to each other. We can plot how the sensitivity and the monopole response function depend on the wave number, as shown in Fig. 9.

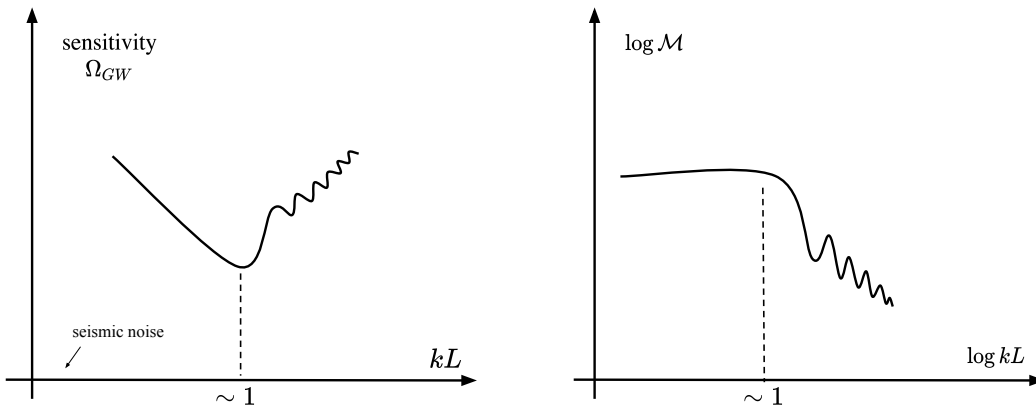


Figure 9: On left, sensitivity of gravitational waves versus kL (length of detector L), given dependence of signal on the correlation $\langle s_{\alpha}^2 \rangle$ through (4.33). For small wavelengths, seismic noise is an obstacle. For large wavelengths, the monopole response oscillates too much. On the right, log-log plot of the monopole detector response versus kL . The detector response drops for $kL \gg 1$ (averaging over many oscillations, see (4.32)), and it is constant for $kL \ll 1$.

For non-isotropic sources, we should repeat the computation and keep $\langle hh \rangle$ in the integral over $d\Omega$. One can search for anisotropies through antenna patterns, see Fig. 10.

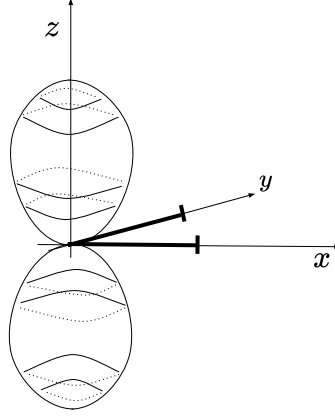


Figure 10: *The interferometer and detector are located at the xy plane. The antenna pattern is a property of the detector and is useful for detecting anisotropy.*

For polarized sources, $P_{\times}(k) \neq P_{+}(k)$, we should repeat the computation and keep $\langle hh \rangle$ in \sum_{λ} . One can search for polarization through the added multipoles.

4.4 Experiments

Here we briefly comment on three different experimental configurations that can probe SGWBs: ground- and space-based interferometers and pulsar timing arrays. See the diagram in Fig. 11.

4.4.1 Ground-based interferometers

LIGO, Virgo, and KAGRA [9, 13] are collaborations based on ground-based interferometers. These interferometers are designed as in Fig. 7. These experiments rely on very large arms. Even so, according to the ratio $\frac{\Delta L}{L} \sim |h_{\mu\nu}| \sim 10^{-21}$, for arms with $L \sim 10^3$ m, we have $\Delta L \sim 10^{-18}$ m. Compare with the proton dimension 10^{-15} m, and notice that the gravitational wave-interferometer must be extraordinarily sensitive!

Take, for instance, a signal whose peak frequency is at $f \sim 100$ Hz, typical for binary mergers, such that $\lambda \sim L \sim \frac{1}{2\pi f} \sim 750$ km. For such wavelength, construction would be impossible. The trick is to use resonant Fabry-Pérot cavities that reduce the required size to $L \sim 3$ km. With such length, it is possible to detect signals from binary mergers, as LIGO-Virgo detected.

From the last subsection, we have seen that a combination of detectors can improve experimental power. Indeed, if one uses two detectors, one can analyze coincidence and cross-correlation; see, for instance, the first claimed gravitational wave detection by LIGO [9]. For three detectors, one can analyze the 3D localization and polarization of isotropic SGWB; see, for instance, [10].

Notice that the smaller the frequency, the larger the arm. This fact limits the sources that a detector can observe.

4.4.2 Space-based interferometers

LISA [7] is the future space-based interferometer to be launched in the early 2030s. The idea is to reproduce the idea behind ground-based interferometers in space. LISA will have three 2.5×10^6

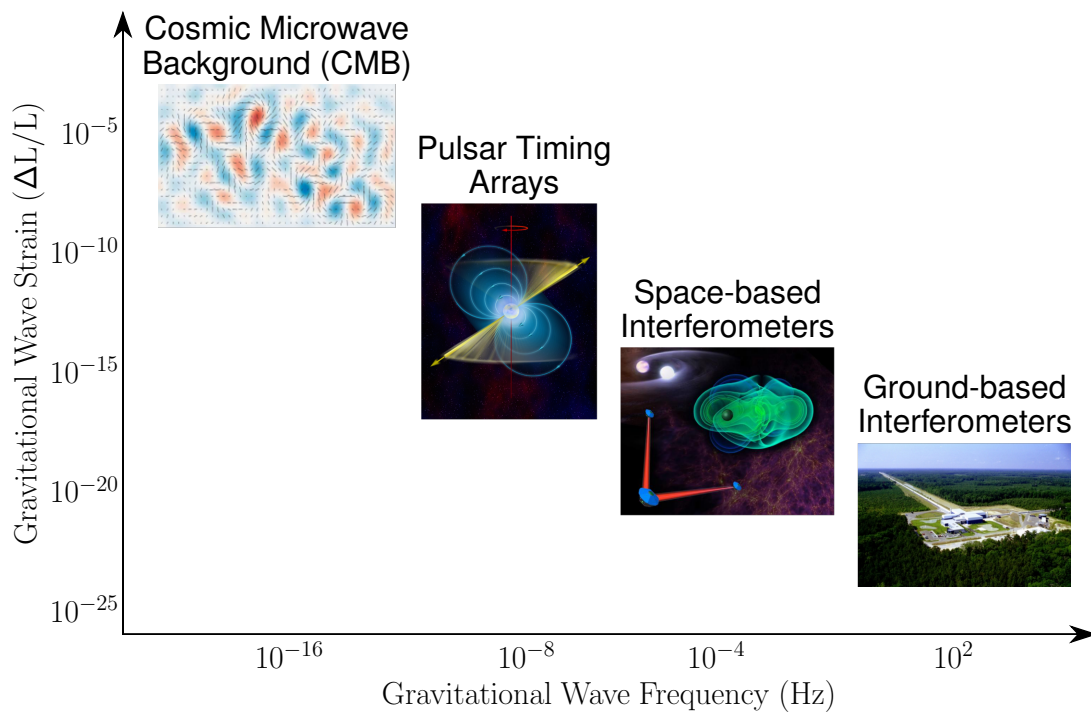


Figure 11: Scheme of different experiments probing the gravitational wave spectrum. Thanks to Michael Lam, from the NANOGrav collaboration, for sharing the code to produce the figure. From left to right, the images are credited to BICEP2, Bill Saxton at NRAO, eLISA, and LIGO, respectively.

km arms that would probe frequencies in the mHz range, with three detectors able to detect two independent signal channels.

This experiment would probe smaller frequencies that, on Earth, would require unrealistic large arms. For such frequencies, it would be possible to detect ultra-compact binaries in our galaxy, supermassive black hole mergers, extreme mass ratio inspirals, and other exotic possibilities. These exotic possibilities are associated with early universe physics associated with SGWB.

4.4.3 Pulsar timing arrays

Pulsar time arrays (PTAs) do not work like the experimental setting described before. Instead, they rely on the detection of gravitational waves by measuring the time of arrival of radio pulses from millisecond pulsars through the spatially correlated fluctuations induced by gravitational waves. PTAs can probe smaller frequencies (in the nHz range) than ground- and space-based interferometers.

As gravitational waves perturb the metric along the Earth-pulsar lines, they modify radio pulses' time of arrival on Earth. A set of PTAs creates correlations across the baselines, while other noise sources are uncorrelated. Searches using PTAs then compare the measured spatial correlations with the expected values from the Helling-Downs curve, a smoking gun for the isotropic, unpolarized background of quadrupole gravitational wave radiation [14].

Supermassive black hole binaries are the main source of gravitational waves at the nHz range. Supermassive black holes have masses larger than 10^5 solar masses, are present in the center of galaxies, and are much heavier than the ones producing the transient signals detected by the LIGO-Virgo collaboration, for instance, [9]. Since the frequency of gravitational waves scales as the inverse of the binary chirp mass, neither LIGO-Virgo nor LISA can detect such supermassive black holes. On top of this astrophysical background, a cosmological background is produced by early-universe and beyond Standard Model physics, which can therefore be probed by PTAs.

NANOGrav [15], PPTA [16], EPTA [17], as well as their joint international consortium IPTA [18] are the largest PTA collaborations. Hints for detection on SGWB were recently claimed by the collaborations [19–22]. They showed statistical evidence for a common-spectrum low-frequency red-noise power-law process (consistent with the expected black hole binary) but without significant evidence for, or against, Helling-Downs correlations. A detection of SGWB can be either confirmed or refuted by coming data releases.

For details on the past, present, and future of PTA collaborations, see, for instance, [23, 24].

5 Lecture: Cosmological sources - Probing beyond Standard Model physics

In the last section, we saw how to compute the energy density ρ_{GW} of gravitational waves, their spectrum Ω_{GW} , the averaged time-delay $\langle s_\alpha^2 \rangle$ for an experimental setting based on interferometers. In this section, we will learn how to characterize frequencies of relic gravitational waves, associating them with cosmological sources.

After presenting a discussion on how gravitational wave detectors can probe different stages of the universe and how we can bind the gravitational wave spectrum with complementary cosmological probes, we discuss primordial sources of gravitational waves [6, 25]. Cosmic gravitational microwave background, phase transitions, and cosmic strings are discussed in this section. Infla-

tion and axion inflation are discussed in Sec. 6.¹⁴

5.1 Characteristic frequencies of relic gravitational waves

If a gravitational wave is emitted with some frequency f_* at time τ_* , then the observed frequency at time τ_0 is red-shifted,

$$f_0 = f_* \frac{a(\tau_*)}{a(\tau_0)}. \quad (5.1)$$

The emitted frequency is given by $f_* = (\epsilon_* H_*^{-1})^{-1}$, where ϵ_* satisfies $\epsilon_* \leq 1$, setting the inverse of Hubble factor $(H_*)^{-1}$ as the cosmological horizon. gravitational waves from a source in the early universe cannot be correlated on time scales larger than $(H_*)^{-1}$, otherwise, it would break causality. The exception is cosmic inflation. The correct value of ϵ_* depends on the source.

Assuming that a gravitational wave signal is produced during the radiation era, $H_*^2 = \frac{\pi^2 g_* T_*^4}{90M_p^4}$, $a \sim 1/T$, $t \sim 1/T^2$, and degrees of freedom $g_* \sim 100$, we have¹⁵

$$f_0 \simeq 10^{-8} \epsilon_*^{-1} \left(\frac{T_*}{\text{GeV}} \right) \text{Hz}, \quad (5.2)$$

$$t_* \simeq 10^{-22} \epsilon_*^{-1} \left(\frac{1\text{Hz}}{f_0} \right)^2 \text{s}. \quad (5.3)$$

Thus, it is possible to associate the observed frequency of gravitational waves in the detectors with the epochs of the universe when such gravitational waves had been produced¹⁶. By operating in different frequency ranges, gravitational wave detectors can probe separated energy scales and cosmological epochs. As we can see in Table 1, in principle we can have access to very high energy scales. These scales cannot be probed by other cosmological probes, for instance, CMB, BBN, and LSS, that can probe temperatures $T_p \leq 1 \text{ MeV}$ ¹⁷.

$\epsilon_* = 1$	f_0 (Hz)	T_* (GeV)
PTA	10^{-8}	0.1
LISA	10^{-2}	10^5
LIGO	10^2	10^9

Table 1: *Typical peak frequencies and their associated temperature of emission, expected for PTAs (pulsar time arrays) and the gravitational wave interferometers LIGO and LISA, for $\epsilon_* = 1$.*

¹⁴We will not discuss scalar-induced gravitational waves, which are related to primordial black holes. See, for example, [26, 27] for discussions on the topic.

¹⁵For inflation, T_* marks re-entry, not inflation scale.

¹⁶The correct correspondence between frequency and temperature of the universe does depend on the relativistic and entropy number of degrees of freedom g_* and $g_{*,S}$, as well as on the equation of the state of the universe. We will not derive a general expression here since it is model-dependent.

¹⁷Take as a grain of salt that the stochastic gravitational wave signal is weak, because of the $1/a^2$ suppression for high-redshift sources.

5.2 Constraints from BBN and CMB

Big bang nucleosynthesis (BBN) and the cosmic microwave background (CMB) are also cosmological probes. They help us to answer the question: “What is the maximum fraction Ω_{GW}/Ω_{rad} we can observe today?”

We start computing $\Delta\rho_{rad} = \rho_{rad}^{obs} - \rho_{rad}^{SM}$, the extra observed radiation due to neutrino species. The energy density due to gravitational waves cannot be larger than $\Delta\rho_{rad}$ itself. After electron decoupling,

$$\rho_{rad} = \rho_\gamma + \rho_\nu = \frac{\pi^2}{30} \left(2 + \frac{7}{4} N_{eff} \left(\frac{4}{11} \right)^{4/3} \right) T^4. \quad (5.4)$$

The factor of 2 corresponds to the two degrees of freedom of photon radiation, $7/4 = (7/8)2$ to neutrinos and anti-neutrinos (fermions with one helicity state each), and $4/11$ to heating of the photon bath relative to the neutrino bath due to e^+e^- decay after neutrino decoupling. N_{eff} is the neutrino effective number given by $N_{eff}^{SM} + \Delta N_{eff}$. In the standard model, $N_{eff}^{SM} = 3.046$. Consequently,

$$\left(\frac{\rho_{GW}}{\rho_\gamma} \right)_{T=MeV} < \frac{\rho_{rad}^{obs} - \rho_{rad}^{SM}}{\rho_\gamma} \leq \frac{7}{8} \left(\frac{4}{11} \right)^{4/3} \Delta N_{eff}. \quad (5.5)$$

At BBN and CMB decoupling, $\Delta N_{eff} \lesssim 0.2$ [28, 29]. Therefore, for $T < (T_{BBN}, T_{CMB})$, the observed ratio is bounded by $\left(\frac{\rho_{GW}}{\rho_\gamma} \right)_T \lesssim 10\%$. Today, $\Omega_\gamma = \frac{\rho_\gamma}{\rho_c} \sim 10^{-5}$, and $\rho_{GW} \lesssim \Omega_\gamma \rho_c \Delta N_{eff}$ constrains the gravitational wave spectrum.

Since, $\rho_{GW} = \rho_c \int d(\log f) \Omega_{GW}(f)$, the BBN constraint implies, for a broad spectrum, that the observed gravitational wave spectrum today is bounded by

$$\Omega_{GW} \lesssim 10^{-6}. \quad (5.6)$$

This constraint holds for gravitational waves inside the horizon at T_{BBN} and T_{CMB} , i.e, the gravitational waves emitted before CMB decoupling. It already constrains some early universe models!

Next, we will focus on different cosmological sources for stochastic gravitational waves.

5.3 Cosmic gravitational microwave background

In the primordial plasma, photon decoupling at $T \sim \text{eV}$ leads to CMB. Likewise, gravitational waves decoupling at $T \sim M_p$ leads to cosmic gravitational microwave background (CGMB) [30]. Because of the very large value of the Planck mass $M_p \sim 10^{18} \text{ GeV}$, it is very hard to detect CGMB:

$$\Omega_{CGMB} \sim \frac{T_{max}}{M_p} \Omega_{CMB}, \quad (5.7)$$

where T_{max} is the highest temperature during radiation domination, at sub-Planckian temperatures, ($T_{max} \leq 10^{16} \text{ GeV}$, approaches BBN bound for $T_{max} \sim M_p$), and Ω_{CMB} is the CMB spectrum observed today. Ω_{CGMB} peaks around to 100 GHz [30], far from any current technology or planned gravitational wave experiment.

5.4 First order phase transitions

First-order phase transitions (PTs) are processes of spontaneous symmetry breaking from a symmetric phase (false vacuum) to a broken phase (true vacuum), as shown in Fig. 12. Bubble col-

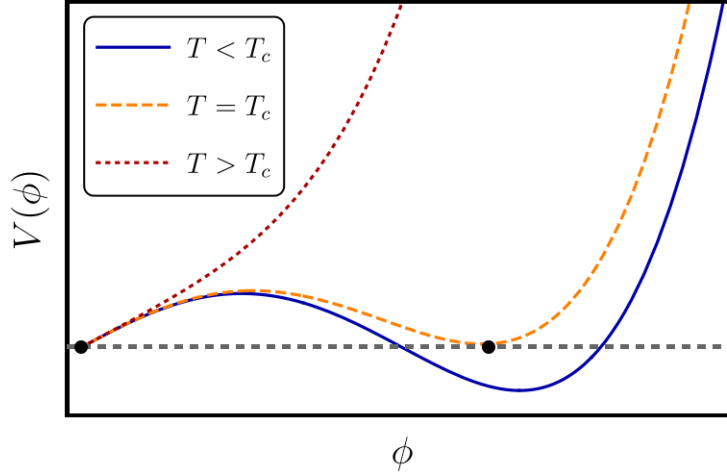


Figure 12: Representation of a first-order phase transition, for a potential $V(\phi)$ depending on a field ϕ (for instance, the Higgs field) and on the temperature T . $\phi = 0$ is the true ground state only for $T > T_c$ (red dotted line). When the temperature decreases, a new local minimum appears, such that at $T = T_c$ both minima are degenerate (orange dashed line). $\phi \neq 0$ is the true ground state for $T < T_c$ (blue solid line). Quantum or thermal fluctuations allow for tunneling between the vacua.

lisions, magneto-hydrodynamics (MHD) turbulence, and sound waves are phenomena sourcing gravitational waves during a 1st order PT.

The peak frequency, for $\epsilon_* \sim 10^{-3}$, is around

$$f_{\text{peak}} \approx 10^{-3} \text{Hz} \left(\frac{T}{100 \text{GeV}} \right), \quad (5.8)$$

where 100 GeV corresponds to the Standard Model (SM) electroweak (EW) phase transition temperature. No signal from the SM EW phase transition is expected because the SM does not have a 1st order PT for the observed Higgs mass [31]. However, several BSM models lead to first-order EW phase transition that could be probed by LISA. From BBN, $\Omega_{GW} \lesssim 10^{-6}$ already constrains some PT models, depending on the strength of the PTs [19].

For more on cosmological phase transitions, see, for instance, the lecture notes [32].

5.5 Cosmic strings

Cosmic strings are one-dimensional topological defects. Topological, or cosmic, defects are products of phase transitions, when the vacuum manifold M is topologically non-trivial, i.e., $\pi_n(M) \neq I$, see [33]. They can be strings ($n = 1$), monopoles ($n = 2$) or textures ($n = 3$) [34]. Let us focus on strings. Here, $\pi_1(M)$ stands for the first homotopy group in a manifold M and counts the number of equivalence classes of loops in M .

Cosmic strings arise in phase transitions if, and only if, for $G \rightarrow H$, $\pi_1(G/H) \neq I$. Cosmic string models are often associated with the spontaneous symmetry breaking of a local U(1) symmetry

in some BSM/grand unified theory (GUT) scenarios. One example is the breaking of $B - L$, the difference between baryon and lepton numbers [35].

The string tension μ is the energy per unit of length. It is related to the amplitude of vacuum expectation value v^2 through $(G\mu) \propto v^2$.

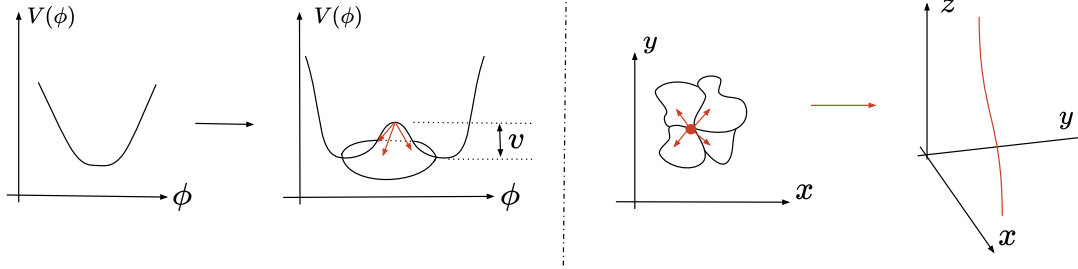


Figure 13: Representation of cosmic strings - one-dimensional topological defects. In the two first plots, we show a complex scalar field potential versus scalar field configuration, where some mechanism allows for a phase transition with a non-vanishing expectation value v . We obtain the two last plots by mapping the solution to real space. In the 2D plot, we show the location of the local extremal point (false vacuum, orange dot) and regions where the scalar field configuration assumes different values; by continuity, these regions intersect each other where the vacuum expectation value $\langle \phi \rangle$ corresponds to the false vacuum. In the 3D plot, we extrapolate the false vacuum region to three spatial dimensions; the reason for the name strings becomes clear.

In the evolution of cosmic string networks, (self-) intersection generates loops. Loops are more energetically favorable, and then there is the emission of particles and gravitational waves by wave excitations of the loops. The scaling regime is a fixed point of this evolution with the property

$$\frac{\rho_{CS}}{\rho_{total}} \approx \text{constant}, \quad (5.9)$$

with $\mathcal{O}(1)$ cosmic strings per Hubble volume¹⁸.

Since it is a continuous process, the spectrum is broader. The gravitational wave signal is characterized by

$$\rho_{GW}(t, f) \propto \sum_{n=1}^{\infty} C_n(f) P_{gw,n}. \quad (5.10)$$

In this expression, $P_{gw,n}$ is the power of a single loop. The larger the string tension μ , the larger P_{gw} . Furthermore, n corresponds to the n -th harmonic, and $C_n(f)$ gives the number of loops emitting gravitational waves, that are observed today at frequency f at time t ,

$$C_n(f) = \frac{2n}{f^2} \int dz \frac{N(l(z), t(z))}{H(z)(1+z)^6}. \quad (5.11)$$

¹⁸This property follows from the fact that in the scaling regime, the only physical scale is the Hubble radius H^{-1} . Therefore, the energy density of cosmic strings $\rho = \mu \times [M]^2 \propto \mu H^2$, while the critical energy density $\rho_{total} = \rho_{crit} = 3H^2/(8\pi G)$, so that the ratio ρ_{CS}/ρ_{total} is constant. This property is essential for cosmic strings phenomenology and it distinguishes strings from monopoles and domain walls. For these defects, the ratio ρ_{CS}/ρ_{total} is not constant and can overclose the universe.

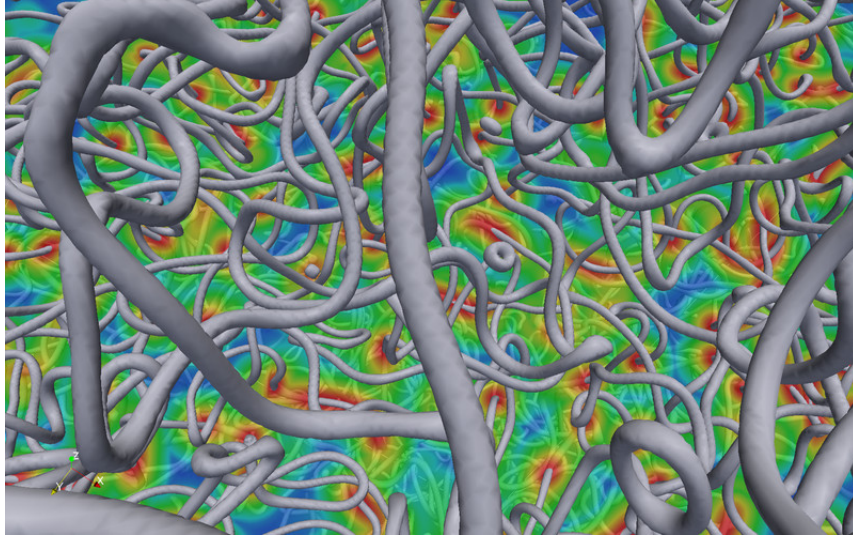


Figure 14: 3D representation of cosmic strings (gray) from a simulation credited to David Daverio, from the group of Professor Martin Kunz, Université de Genève, using simulation data obtained at the Swiss National Supercomputer Centre.

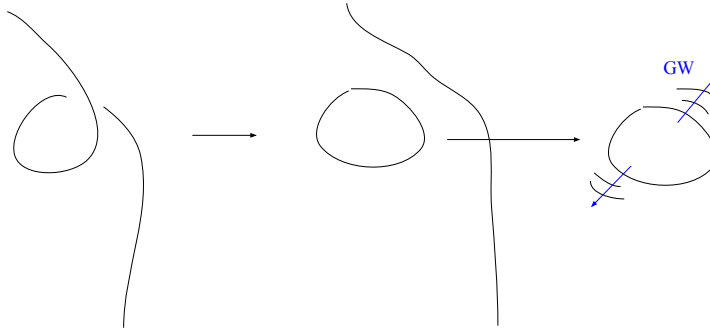


Figure 15: Representation of gravitational waves emitted by loops from cosmic string networks.

Above, the denominator $H(z)(1+z)^6$ tells about the cosmological history. $N(l(z), t(z))$ is the number of loops of length l at time t , where the length l is given by $l = 2n/(f(1+z))$. The computation is not straightforward and there are different methods. In order to solve this integral analytically, the usual assumption is loops being sourced with $lH = \alpha = \text{constant}$. Numerically, see, for instance, [36].

There are two general properties: the larger $G\mu$, the stronger Ω_{GW} ; the higher the gravitational wave characteristic frequency, the earlier the emission. Moreover, gravitational wave signals constrain the string tension and bound the symmetry-breaking scale. Large symmetry-breaking scales for topologically stable cosmic strings were excluded by PTAs:

$$G\mu \lesssim 10^{-10} \rightarrow \nu \lesssim 10^{14} \text{ GeV}.$$

These signals are associated with a largely flat spectrum at high frequencies and with a mild peak at nHz-mHz frequencies, as shown in Fig. 16.

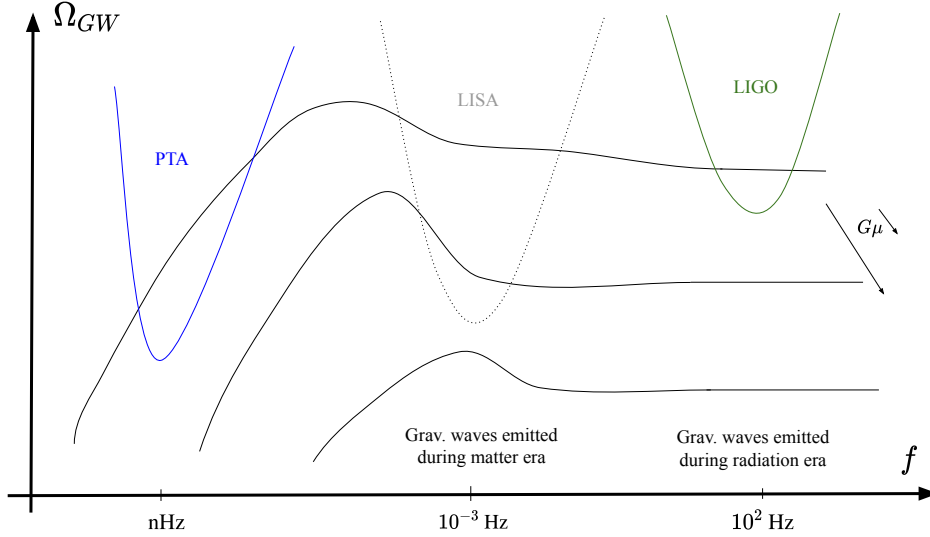


Figure 16: Amplitude of gravitational waves generated by cosmic strings, with different string tensions μ , as a function of frequency. The larger $G\mu$, the larger the amplitude Ω_{GW} . We also plot the frequency range probed, or expected to be probed, by LIGO, LISA, and PTA collaborations. PTA signals already constrain cosmic string models with large $G\mu$, whose frequency peak is at the nHz scale.

Finally, as a note on possible production mechanisms, the SM cannot produce strings, but BSM theories, such as grand unification theories (GUTs), can. Complementary to collider searches, gravitational waves can probe GUT physics. For instance, in some GUT models, strings can decay via monopole pair production, suppressing Ω_{GW} at low f . *Metastable defects* relies on a sequence of phase transitions [37]

$$G \rightarrow G' \rightarrow SM, \quad \pi_n(G/SM) = \mathbb{I} \quad \text{and} \quad \pi_n(G/G') \neq \mathbb{I}, \pi_m(G'/SM) \neq \mathbb{I} \quad (5.12)$$

i.e. the manifolds (G/G') and (G'/SM) have non-trivial homotopy groups, but the homotopy group of (G/SM) is trivial so that the defect is not topologically stable.

For example, we have the symmetry groups $G = SO(10)$ and $G' = U(1)/SM$. $G \rightarrow G'$ generates monopoles, $G' \rightarrow SM$ generates cosmic strings, but $\pi_1(SO(10)/SM) = \mathbb{I}$. Therefore, strings are not topologically stable, thus metastable. There are at least two decaying mechanisms. In the first mechanism, there is an initial population of monopoles and strings; then, the *string-monopole gas* decays fast. In a second mechanism, relevant if inflation dilutes away the initial monopole population, strings can only decay via spontaneous Schwinger monopole production with a decay rate $\propto e^{-m^2/\mu}$, where m is the monopole mass; then, these *metastable strings* can emit gravitational waves [38]. At low frequencies, the spectrum is suppressed, and it cannot be excluded by the PTA bounds while allowing for larger spectra at larger frequencies, which opens a discovery space for LIGO [39].

6 Lecture: Gravitational waves from axion inflation

In the last section, we learned how to characterize stochastic backgrounds and described primordial sources associated with beyond-standard model physics. In this section, we describe another potential source of gravitational wave backgrounds: inflation. We focus on the single field slow-roll inflation and on an axion-like inflaton particle coupled to a photon.

6.1 Cosmic inflation

From the Einstein equations ($M_p = 1, c = 1$),

$$R_{\mu\nu} - \frac{1}{2}Rg_{\mu\nu} = T_{\mu\nu}, \quad (6.1)$$

for a FRW spacetime, the Friedmann equations are:

$$\left(\frac{\dot{a}}{a}\right)^2 = H^2 = \frac{\rho}{3} - \frac{k}{a^2}, \quad (6.2)$$

$$\frac{\ddot{a}}{a} = \dot{H} + H^2 = -\frac{1}{6}(\rho + 3p), \quad (6.3)$$

for a perfect fluid given by $T^\mu{}_\nu = \text{diag}(\rho, -p, -p, -p)$, where ρ is the energy density and p is the pressure, and $H = H(t)$ is the Hubble parameter. On the one hand, we have decelerated expansion $\ddot{a} < 0$ if the equation of state parameter is $\omega = p/\rho > -1/3$. On the other hand, there are two problems associated with decelerated expansion: the horizon and flatness problems¹⁹. Therefore, the condition $\omega < -1/3$ must be satisfied by a cosmic inflation model, that took place in the universe before BBN.

Consider a **single-field slow-roll** model ($M_p, c = 1$):

$$S = \int d^4x \sqrt{-g} \left(\frac{R}{2} - \frac{1}{2}g^{\mu\nu} \partial_\mu \phi \partial_\nu \phi - V(\phi) \right). \quad (6.4)$$

The energy-momentum tensor is given by²⁰

$$T_{\mu\nu}^{(\phi)} = -\frac{2}{\sqrt{-g}} \frac{\delta S_\phi}{\delta g^{\mu\nu}} = \partial_\mu \phi \partial_\nu \phi - g_{\mu\nu} \left(\frac{1}{2} \partial_\alpha \phi \partial^\alpha \phi + V(\phi) \right) \quad (6.5)$$

By assuming that the field is homogeneous, i.e. $\phi(x, t) = \phi(t)$, $\partial_i \phi = 0$, we have

$$\rho_\phi = \frac{\dot{\phi}^2}{2} + V(\phi), \quad p_\phi = \frac{\dot{\phi}^2}{2} - V(\phi), \quad (6.6)$$

and then

$$\omega_\phi = \frac{p_\phi}{\rho_\phi} = \frac{\dot{\phi}^2/2 - V(\phi)}{\dot{\phi}^2/2 + V(\phi)} \Rightarrow \omega_\phi \rightarrow -1 \quad \text{if} \quad V(\phi) \gg \dot{\phi}^2/2. \quad (6.7)$$

¹⁹The horizon problem is due to the fact that the Hubble horizon grows faster than any other physical scale so that the observed CMB spectrum implies uniformity for regions that were not causally connected in the early universe. The flatness problem is about the fact that the curvature of the universe is very small today, which would require even smaller curvatures in the past. For more details on these problems, see, for instance, the lecture notes on inflation [40].

²⁰Our convention is $g_{\mu\nu} = \bar{g}_{\mu\nu} + h_{\mu\nu}$, where $\bar{g}_{\mu\nu} = \text{diag}(-1, a, a, a)$.

The last condition is known as slow-roll, see Fig. 17, and therefore this model is able to describe inflation, since $\omega_\phi < -1/3$. In particular, from the Friedmann equations, its solution is de-Sitter, i.e. an exponential expansion $a(t) \propto e^{Ht}$, for a constant positive Hubble parameter H .

For the scalar field ϕ , the equation of motion is

$$\frac{1}{\sqrt{-g}} \partial_\mu (\sqrt{-g} \partial^\mu \phi) + V_{,\phi} = 0 \quad \Rightarrow \quad \ddot{\phi} + 3H\dot{\phi} + V_{,\phi} = 0, \quad (6.8)$$

for homogeneous ϕ with $H^2 = \frac{1}{3}(\dot{\phi}^2/2 + V(\phi)) \approx \frac{V(\phi)}{3}$.

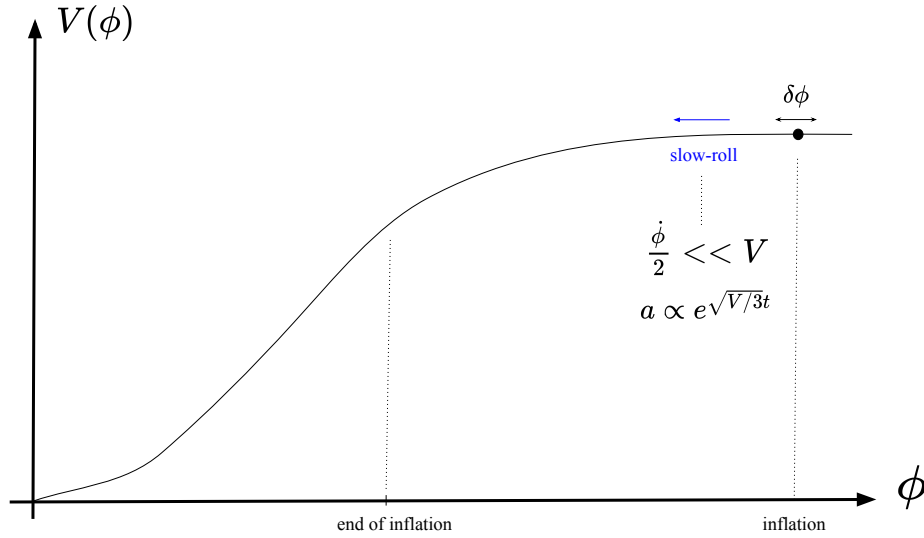


Figure 17: *Slow-roll scalar field potential $V(\phi)$ as a function of ϕ . Slow-roll condition implies that the potential does not vary much with the evolution of the field, allowing for accelerating solutions $\omega < -1/3$. In the evolution of the scalar field, time runs from right to left. At the beginning of the evolution, $V(\phi) \gg \dot{\phi}^2$, implies a constant $H = \sqrt{V/3}$ and a de-Sitter solution for the scale factor. In addition, quantum fluctuations $\delta\phi$ source density scalar perturbations. Inflation ends when the slow-roll condition is not satisfied.*

In addition, quantum fluctuations $\delta\phi$ and $\delta g^{\mu\nu}$ source density perturbations and gravitational waves. Fluctuations only propagate after horizon re-entry since they are frozen in the super-horizon, as discussed in Sec. 4.2. See Fig. 18. Next, we focus on the tensor perturbation.

6.2 gravitational waves from inflation

The field equations in vacuum are given in Sec. 4,

$$\tilde{h}_\lambda''(\mathbf{k}, \tau) + \left(k^2 + \frac{a''}{a}\right) \tilde{h}_\lambda(\mathbf{k}, \tau) = 0, \quad (6.9)$$

for $\tilde{h}_\lambda = ah_\lambda$, for the two polarization modes. At $\tau \rightarrow -\infty$, we have the Bunch-Davies vacuum solution

$$\lim_{\tau \rightarrow -\infty} \tilde{h}_\lambda = \frac{2e^{-ik\tau}}{\sqrt{2k}}, \quad (6.10)$$

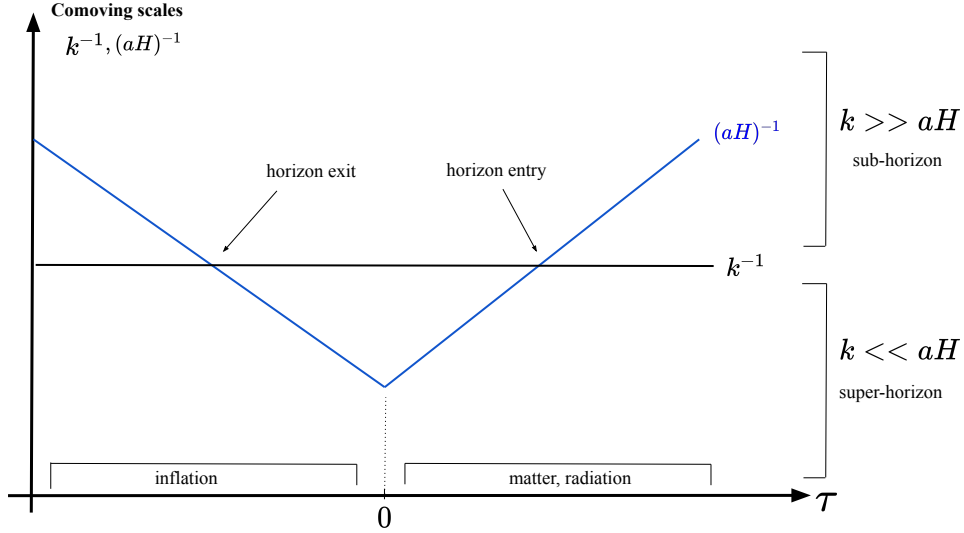


Figure 18: Diagram of the comoving scales k^{-1} and $(aH)^{-1}$ as a function of conformal time, normalized so that inflation ends at $\tau = 0$. For a mode with a given wave number k , at earlier times during inflation, the Hubble horizon H is constant and the scale factor $a(t)$ grows exponentially. As a result, $(aH)^{-1}$ decreases, so that the mode leaves the horizon when $k^{-1} = (aH)^{-1}$. After inflation, for both matter and radiation eras, $(aH) \sim 1/t$, and $(aH)^{-1}$ increases with time so that the mode re-enters the horizon when $k^{-1} = (aH)^{-1}$. Sub-horizon scales refer to modes in the horizon $k^{-1} < (aH)^{-1}$. Super-horizon scales refer to modes out of the horizon $k^{-1} > (aH)^{-1}$.

so that

$$\tilde{h}_\lambda = \frac{2e^{-ik\tau}}{\sqrt{2k}} \left(1 - \frac{i}{k\tau} \right) \quad (6.11)$$

and

$$\langle h_\lambda(\mathbf{k}) h_{\lambda'}(\mathbf{k}') \rangle = (2\pi)^3 \delta_{\lambda\lambda'} \delta^3(\mathbf{k} - \mathbf{k}') \left(\frac{1}{M_p} \right) \frac{|\tilde{h}_\lambda|^2}{a^2} \quad (6.12)$$

gives us

$$\frac{|\tilde{h}_\lambda|^2}{a^2} = \frac{4}{a^2(2k)} \left(1 + \frac{1}{k^2\tau^2} \right) = \frac{4H^2}{2k^3} (1 + k^2\tau^2), \quad (6.13)$$

for the de-Sitter expanding universe solution, where $aH = -1/\tau$. The last term above can be neglected on super horizon scales, since $(aH)^{-1} < k^{-1}$. We have

$$\langle h_\lambda(\mathbf{k}) h_{\lambda'}(\mathbf{k}') \rangle = (2\pi)^3 \delta_{\lambda\lambda'} \delta^3(\mathbf{k} - \mathbf{k}') \left(\frac{2}{M_p} \right)^2 \frac{H_*^2}{2k^3}, \quad (6.14)$$

where $H_* = H(k\tau = 1)$ is the Hubble parameter when the mode k leaves the horizon during inflation. Since gravitational waves are frozen on super-horizon scales and inflation ends before horizon re-entry, the last imprint from inflation in the gravitational wave signal comes from the time when the mode leaves the horizon. From (6.14), we get the power spectrum

$$P_h(k) = \left(\frac{2}{M_p} \right)^2 \frac{H_*^2}{2k^3}. \quad (6.15)$$

Slow-roll condition implies $H \approx \text{constant}$ and a scale-invariant spectrum $\Delta_t^2 \propto k^3 P_h(k) = \text{constant}$. How large are these tensor perturbations? CMB observations point to a tensor-to-scalar ratio $r = \Delta_t/\Delta_s < 0.1$ [29]. With Δ_s measured, the upper bound on r is an upper bound on Δ_t and hence on the gravitational wave signal. This would imply $\Omega_{GW} \leq 10^{-15}$, which is too small for PTAs, LISA, and LIGO to detect a signal.

For more details on gravitational waves from inflation, see for instance the review [41].

6.3 Axion inflation

Although the previous slow-roll scalar field model is the dominant paradigm in inflation cosmology, the requirement of having a flat scalar potential is a challenge in particle physics. We can solve this problem by introducing symmetry, which protects the flatness of the potential. One simple implementation is to assume that the inflaton ϕ is a pseudo-Nambu-Goldstone boson, whose model is invariant under *shift symmetry*: $\phi \rightarrow \phi + c$, where c is a constant. The resulting pseudo-scalar field model is an axion-like particle model:

$$S = \int d^4x \left\{ \sqrt{-g} \left[\frac{R}{2} - \frac{1}{2} \partial_\mu \phi \partial^\mu \phi - V(\phi) - \frac{1}{4} F_{\mu\nu} F^{\mu\nu} \right] - \frac{\phi}{4\pi\bar{f}} F_{\mu\nu} \tilde{F}^{\mu\nu} \right\}, \quad (6.16)$$

where $F_{\alpha\beta} = \partial_\alpha A_\beta - \partial_\beta A_\alpha$, $\tilde{F}^{\mu\nu} = 1/2 \epsilon^{\mu\nu\alpha\beta} F_{\alpha\beta}$ is the dual strength tensor, and the inflaton ϕ is coupled to the (dark) photon through a dimension five operator and the coupling $1/\bar{f}$. Shift symmetry²¹ protects the flatness of $V(\phi)$, in the sense that symmetry breaking means departure of the flatness of the potential.

Next, we derive the equations of motion for A_μ , ($d\tau = a dt$)

$$\square \vec{A} = -\vec{A}'' + \nabla^2 \vec{A} = -\frac{\phi'}{\pi\bar{f}} \nabla \times \vec{A}, \quad (6.17)$$

for the gauge-fixing $\nabla \cdot \vec{A} = 0$ and $A_0 = 0$. The right-hand side contains the axion-like particle term and is interpreted as a source term. With the Fourier decomposition

$$\vec{A}(\tau, \vec{x}) = \sum_{\lambda=\pm} \int \frac{d^3k}{(2\pi)^{3/2}} \left(A_\lambda(\tau, \vec{k}) \vec{\varepsilon}_\lambda(\vec{k}) \hat{a}_\lambda(\vec{k}) e^{i\vec{k}\cdot\vec{x}} + \text{h.c.} \right), \quad (6.18)$$

polarization vectors

$$\vec{\varepsilon}_\lambda(\vec{k}) \cdot \vec{\varepsilon}_{\lambda'}(\vec{k}) = \delta_{\lambda\lambda'}, \quad \vec{\varepsilon}_\lambda(\vec{k}) \cdot \vec{k} = 0, \quad i\vec{k} \times \varepsilon_\lambda(\vec{k}) = \lambda k \varepsilon_\lambda(\vec{k}), \quad (6.19)$$

and creation and annihilation operators that satisfy $[\hat{a}_\lambda(\vec{k}), \hat{a}_{\lambda'}^\dagger(\vec{k}')] = \delta_{\lambda\lambda'} \delta^{(3)}(\vec{k} - \vec{k}')$, the equations of motion are

$$\left[\frac{\partial^2}{\partial \tau^2} + k^2 \left(1 \mp \frac{2\xi}{k\tau} \right) \right] A_\pm(\tau, k) = 0, \quad \xi = \frac{\dot{\phi}}{2\pi\bar{f}H}. \quad (6.20)$$

Assuming Bunch-Davies vacuum at $\tau \rightarrow -\infty$, the solutions are

$$A_\lambda^k(\tau) = \frac{e^{\lambda\pi\xi/2}}{\sqrt{2k}} W_{-i\lambda\xi, 1/2}(2ik\tau), \quad (6.21)$$

²¹The last term of the action can be rewritten as $\phi F_{\mu\nu} \tilde{F}^{\mu\nu} = 2\phi \partial_\mu (\epsilon^{\mu\nu\alpha\beta} A_\nu \partial_\rho A_\sigma) = -2\partial_\mu \phi (\epsilon^{\mu\nu\alpha\beta} A_\nu \partial_\rho A_\sigma)$, which makes it explicitly shift-symmetric.

where we have used a Whittaker W function. There is tachyonic instability²² for $A_+(\dot{\phi} > 0)$ if $-k\tau = k(aH)^{-1} < 2\xi$. In this case, there is exponential gauge field production for $A_+(\dot{\phi} > 0)$ when $(aH)^{-1} \sim k^{-1}$, i.e., around horizon exit (assuming $\xi \sim \mathcal{O}(1)$). Therefore, this production can overcome the exponential de-Sitter expansion, which dilutes matter/radiation. This way, this mechanism can provide a visible signal. The largest contribution is at the end of inflation since $\xi \sim \dot{\phi}$ grows, as ϕ rolls down its potential, see Fig. 19.

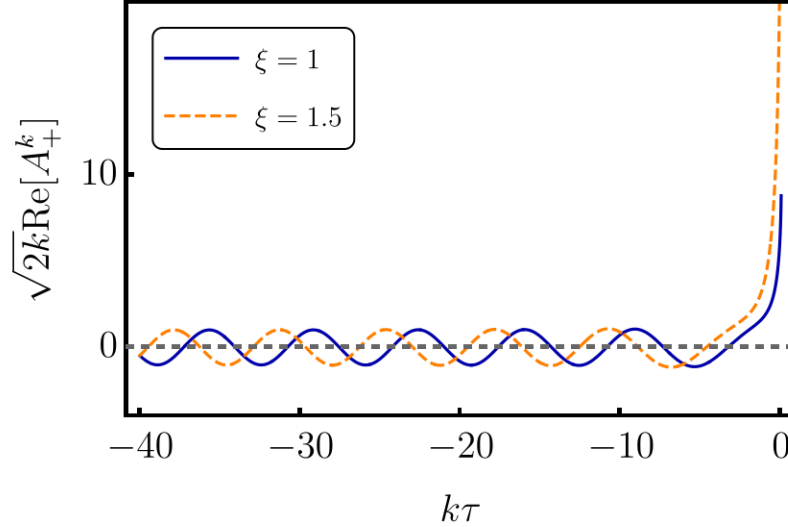


Figure 19: Exponential gauge field production for the $A_+(\xi > 0)$ solution at around horizon exit. The larger ξ , the larger the gauge field production.

Next, we describe the gravitational wave signal from axion inflation. The field equations from (6.16) for the rank-2 tensor are²³

$$h''_{ij}(\mathbf{x}, \tau) + \frac{2a'}{a} h'_{ij}(\mathbf{x}, \tau) - \nabla^2 h_{ij}(\mathbf{x}, \tau) = 2\Pi_{ij}{}^{ab} T_{ab}, \quad (6.22)$$

whose solution is

$$h_{ij}(\vec{k}, \tau) = 2 \int d\tau' G_k(\tau, \tau') \Pi_{ij}{}^{ab} T_{ab}, \quad (6.23)$$

where the Green functions satisfy $[\partial_\tau^2 + 2a'/a \partial_\tau + k^2]G_k = 0$, $\Pi_{ij}{}^{ab}$ is the traceless and transverse projection operator, and T_{ab} is the energy-momentum tensor from the axion-like particle model. By using the solution A_+ from (6.21) in T_{ab} , we can compute the contribution for the gravitational wave spectrum.

Since $\xi \propto \dot{\phi}$, and ϕ is a pseudo-scalar field, we have parity violation. The chiral contribution is a consequence of the enhancement of only the A_+ mode above. Indeed, we have two helicities (h_+ and h_-) whose contributions to the gravitational wave spectrum are different. The larger

²²In other contexts, tachyons are associated with space-like propagations (propagation speed larger than the speed of light). We highlight that in these notes, this is **not** what we mean by tachyonic instability. Instead, we mean a real exponential solution for the differential equation (6.20), which leads to the amplification of the mode A_+ .

²³See details on [42].

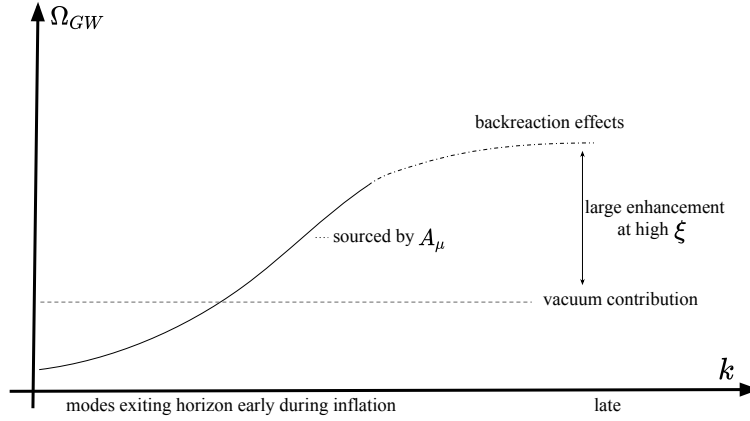


Figure 20: *gravitational wave spectrum for the axion-inflaton model. The vacuum contribution accounts for inflationary gravitational waves without a source. Larger wavelengths exit the horizon earlier frozen and contribute less to the spectrum. But there is also a large enhancement of gauge boson production, due to ξ . Then, the precise balance requires taking into account the back-reaction of the gauge boson onto the axion field.*

contribution to the spectrum is

$$\Omega_{GW} = \left(\frac{H}{\pi M_p} \right)^2 \left(1 + 10^{-7} \frac{H^2}{M_p^2} \frac{e^{4\pi\xi}}{\xi^6} \right). \quad (6.24)$$

The first term corresponds to the vacuum contribution (solution of the homogeneous equation (6.20), without source, computed in the previous sections) and the second term is sourced by A_μ . This last contribution is chiral, and its signature can be probed by LISA, the third-generation Einstein telescope, and the Cosmic Explorer detectors by searching for anisotropies. For the LIGO-Virgo-KAGRA (LVK) collaboration, see [43].

The gravitational wave spectrum can be seen in Fig. 20. There is a large enhancement for large values of ξ due to the exponential production, and back-reaction effects from the gauge bosons onto the axion field become important [44].

The perturbations sourced by the gauge field can be probed by CMB observations, searches for primordial black holes, and gravitational wave experiments (PTAs, LISA, and LVK). In particular, in this model, the spectrum will be peaked towards higher frequencies, corresponding to modes exiting the horizon just before the end of inflation. More details on axion inflation can be found, for instance, in [25, 45].

7 Conclusions

In these lecture notes on gravitational waves from the early universe, we derived the main generic property of gravitational waves, introduced the stochastic gravitational waves, discussed ongoing and future detection efforts, and summarized some primordial sources of gravitational waves.

We started with the basics in the first lecture, with the derivation of the Einstein equations for a linear perturbed metric $g_{\mu\nu} = \eta_{\mu\nu} + h_{\mu\nu}$. We evaluated the degrees of freedom of the linearized metric tensor and fixed all the nonphysical degrees of freedom. The solution of the Einstein

equation for a gravitational wave in a vacuum is a sine wave. Hence, any test mass, while a gravitational wave is passing by, will follow a sinusoidal geodesic. This effect on test masses is the gist of gravitational wave measurement.

In the second lecture, we derived the gravitational wave emitted by a source given by an energy-momentum tensor $T_{\mu\nu}$ and showed that gravitational waves carry energy that curves the background. An important aspect of this section is the distinction between gravitational radiation and the curved background. The power of gravitational radiation was given by Einstein's quadrupole formula in the last part of this lecture.

In the third lecture, we introduced stochastic gravitational wave backgrounds (SGWBs). These backgrounds are defined as the superposition of gravitational waves with different wave numbers \mathbf{k} (both in magnitude and direction), coming from all directions in the sky. We derived their main properties. Since these waves behave like noise, it is a challenge to detect them. Although we have never detected SGWBs, boosted by the detection of gravitational waves (transient signal) by the LIGO-Virgo collaboration, a new generation of experiments (ground-based, space-based, and pulsar time arrays) expect to detect stochastic signals in the near future. We briefly discussed experimental efforts in this direction.

SGWBs can have astrophysical and/or cosmological origins. The astrophysical sources of SGWBs are supermassive black-hole binaries. A detection of astrophysical SGWBs would confirm again a prediction of General Relativity, now for a different range of masses, never probed before. In a binary merger, the larger the black hole masses, the lower the frequencies of the gravitational waves emitted. Pulsar time arrays collaborations expect to detect such signals.

On top of this astrophysical background, there are also cosmological sources from the early universe. These primordial sources produced gravitational waves way before the emission of Cosmic Microwave Background (CMB) and these waves traveled freely through the hot plasma of the early universe. Since beyond Standard Model (BSM) physics relies on mechanisms in energy scales beyond the ones current accelerators can probe, the phenomenology of SGBWs from the early universe is an important step towards probing BSM physics. In this context, in the fourth lecture, we first discussed how we can use data from gravitational waves as complimentary probes to CMB and BBN bounds to constrain beyond Standard Model physics and the earlier stages of the universe. Then, we discussed how first-order phase transitions and cosmic strings, and, in the fifth lecture, how inflation and axion inflation contribute to the gravitational wave spectrum.

Data from gravitational waves, therefore, opens a new window to the phenomenology of new physics and can give important insights into new physics. In the next decade, we expect the development of detection techniques and prospects for the detection of cosmological sources from different collaborations, such as LVK, LISA, PTAs, SKA, the Einstein telescope, and the Cosmic Explorer. Better stay tuned!

We highlight that these notes at any moment intend to substitute the extensive literature on gravitational waves and the cosmological sources presented here. Instead, we believe our notes can be seen as an introduction or even as an executive summary of the field, where we highlighted some of the main cosmological sources and the main results available in the literature for each one of the sources.

Acknowledgements

We thank all the organizers and students for the friendly and productive atmosphere in the 27th W.E. Heraeus Summer School "Saalburg" for Graduate Students on "Foundations and New Methods in Theoretical Physics". We thank Dr. Valerie Domcke for allowing us to use her lecture notes as the starting point of this work. R.R.L.d.S. thanks Tobias Schröder for feedback on the manuscript and Professor Kai Schmitz and his group at ITP, WWU Münster, for discussions and hospitality during the last stages of preparation of these notes.

Author contributions These lecture notes are based on lectures given by Valerie Domcke. The notes were written up by Rafael R. Lino dos Santos and Linda M. van Manen.

Funding information R.R.L.d.S. is supported by a research grant (29405) from VILLUM FONDEN. L.M.v.M is supported by the Volkswagen Foundation.

References

- [1] M. Maggiore, *Gravitational Waves. Vol. 1: Theory and Experiments*, Oxford Master Series in Physics. Oxford University Press, ISBN 978-0-19-857074-5, 978-0-19-852074-0 (2007).
- [2] S. Carroll, *Spacetime and Geometry. An introduction to general relativity*, Pearson Education Limited, ISBN 978-1-292-02663-3 (2014).
- [3] D. Baumann, *TASI Lectures on Inflation*, doi:[10.48550/arXiv.0907.542](https://doi.org/10.48550/arXiv.0907.542) (2012).
- [4] C. Caprini and D. G. Figueroa, *Cosmological Backgrounds of Gravitational Waves*, *Class. Quant. Grav.* **35**(16), 163001 (2018), doi:[10.1088/1361-6382/aac608](https://doi.org/10.1088/1361-6382/aac608), [1801.04268](https://arxiv.org/abs/1801.04268).
- [5] N. Christensen, *Stochastic Gravitational Wave Backgrounds*, *Rept. Prog. Phys.* **82**(1), 016903 (2019), doi:[10.1088/1361-6633/aae6b5](https://doi.org/10.1088/1361-6633/aae6b5), [1811.08797](https://arxiv.org/abs/1811.08797).
- [6] R. Caldwell *et al.*, *Detection of early-universe gravitational-wave signatures and fundamental physics*, *Gen. Rel. Grav.* **54**(12), 156 (2022), doi:[10.1007/s10714-022-03027-x](https://doi.org/10.1007/s10714-022-03027-x), [2203.07972](https://arxiv.org/abs/2203.07972).
- [7] P. Amaro-Seoane *et al.*, *Laser Interferometer Space Antenna*, arXiv e-prints (2017), [1702.00786](https://arxiv.org/abs/1702.00786).
- [8] B. P. Abbott *et al.*, *Exploring the Sensitivity of Next Generation Gravitational Wave Detectors*, *Class. Quant. Grav.* **34**(4), 044001 (2017), doi:[10.1088/1361-6382/aa51f4](https://doi.org/10.1088/1361-6382/aa51f4), [1607.08697](https://arxiv.org/abs/1607.08697).
- [9] B. P. Abbott *et al.*, *Observation of Gravitational Waves from a Binary Black Hole Merger*, *Phys. Rev. Lett.* **116**(6), 061102 (2016), doi:[10.1103/PhysRevLett.116.061102](https://doi.org/10.1103/PhysRevLett.116.061102), [1602.03837](https://arxiv.org/abs/1602.03837).
- [10] B. P. Abbott *et al.*, *GW170817: Observation of Gravitational Waves from a Binary Neutron Star Inspiral*, *Phys. Rev. Lett.* **119**(16), 161101 (2017), doi:[10.1103/PhysRevLett.119.161101](https://doi.org/10.1103/PhysRevLett.119.161101), [1710.05832](https://arxiv.org/abs/1710.05832).

- [11] V. Domcke, *Matter, Dark Matter and Gravitational Waves from a GUT-Scale $U(1)$ Phase Transition*, Ph.D. thesis, Hamburg U., doi:[10.3204/DESY-THESIS-2013-037](https://doi.org/10.3204/DESY-THESIS-2013-037) (2013).
- [12] L. S. Finn, S. L. Larson and J. D. Romano, *Detecting a Stochastic Gravitational-Wave Background: The Overlap Reduction Function*, Phys. Rev. D **79**, 062003 (2009), doi:[10.1103/PhysRevD.79.062003](https://doi.org/10.1103/PhysRevD.79.062003), [0811.3582](https://arxiv.org/abs/0811.3582).
- [13] T. Akutsu *et al.*, *Overview of KAGRA : KAGRA science*, arXiv e-prints (2020), [2008.02921](https://arxiv.org/abs/2008.02921).
- [14] F. A. Jenet and J. D. Romano, *Understanding the gravitational-wave Hellings and Downs curve for pulsar timing arrays in terms of sound and electromagnetic waves*, Am. J. Phys. **83**, 635 (2015), doi:[10.1119/1.4916358](https://doi.org/10.1119/1.4916358), [1412.1142](https://arxiv.org/abs/1412.1142).
- [15] A. Brazier *et al.*, *The NANOGrav Program for Gravitational Waves and Fundamental Physics* (2019), [1908.05356](https://arxiv.org/abs/1908.05356).
- [16] M. Kerr *et al.*, *The Parkes Pulsar Timing Array project: second data release*, Publ. Astron. Soc. Austral. **37**, e020 (2020), doi:[10.1017/pasa.2020.11](https://doi.org/10.1017/pasa.2020.11), [2003.09780](https://arxiv.org/abs/2003.09780).
- [17] G. Desvignes *et al.*, *High-precision timing of 42 millisecond pulsars with the European Pulsar Timing Array*, Mon. Not. Roy. Astron. Soc. **458**(3), 3341 (2016), doi:[10.1093/mnras/stw483](https://doi.org/10.1093/mnras/stw483), [1602.08511](https://arxiv.org/abs/1602.08511).
- [18] B. B. P. Perera *et al.*, *The International Pulsar Timing Array: Second data release*, Mon. Not. Roy. Astron. Soc. **490**(4), 4666 (2019), doi:[10.1093/mnras/stz2857](https://doi.org/10.1093/mnras/stz2857), [1909.04534](https://arxiv.org/abs/1909.04534).
- [19] Z. Arzoumanian *et al.*, *The NANOGrav 12.5 yr Data Set: Search for an Isotropic Stochastic Gravitational-wave Background*, Astrophys. J. Lett. **905**(2), L34 (2020), doi:[10.3847/2041-8213/abd401](https://doi.org/10.3847/2041-8213/abd401), [2009.04496](https://arxiv.org/abs/2009.04496).
- [20] B. Goncharov *et al.*, *On the Evidence for a Common-spectrum Process in the Search for the Nanohertz Gravitational-wave Background with the Parkes Pulsar Timing Array*, Astrophys. J. Lett. **917**(2), L19 (2021), doi:[10.3847/2041-8213/ac17f4](https://doi.org/10.3847/2041-8213/ac17f4), [2107.12112](https://arxiv.org/abs/2107.12112).
- [21] A. Chalumeau *et al.*, *Noise analysis in the European Pulsar Timing Array data release 2 and its implications on the gravitational-wave background search*, Mon. Not. Roy. Astron. Soc. **509**(4), 5538 (2021), doi:[10.1093/mnras/stab3283](https://doi.org/10.1093/mnras/stab3283), [2111.05186](https://arxiv.org/abs/2111.05186).
- [22] J. Antoniadis *et al.*, *The International Pulsar Timing Array second data release: Search for an isotropic gravitational wave background*, Mon. Not. Roy. Astron. Soc. **510**(4), 4873 (2022), doi:[10.1093/mnras/stab3418](https://doi.org/10.1093/mnras/stab3418), [2201.03980](https://arxiv.org/abs/2201.03980).
- [23] S. R. Taylor, *The Nanohertz Gravitational Wave Astronomer* (2021), [2105.13270](https://arxiv.org/abs/2105.13270).
- [24] A. I. Renzini, B. Goncharov, A. C. Jenkins and P. M. Meyers, *Stochastic Gravitational-Wave Backgrounds: Current Detection Efforts and Future Prospects*, Galaxies **10**(1), 34 (2022), doi:[10.3390/galaxies10010034](https://doi.org/10.3390/galaxies10010034), [2202.00178](https://arxiv.org/abs/2202.00178).
- [25] P. Auclair *et al.*, *Cosmology with the Laser Interferometer Space Antenna* (2022), [2204.05434](https://arxiv.org/abs/2204.05434).
- [26] G. Domènech, *Scalar Induced Gravitational Waves Review*, Universe **7**(11), 398 (2021), doi:[10.3390/universe7110398](https://doi.org/10.3390/universe7110398), [2109.01398](https://arxiv.org/abs/2109.01398).

- [27] V. De Luca, *Signals from the Early Universe: Black Holes, Gravitational Waves and Particle Physics*, Ph.D. thesis, Geneva U., Dept. Theor. Phys., doi:[10.13097/archive-ouverte/unige:162100](https://doi.org/10.13097/archive-ouverte/unige:162100) (2022), [2207.08638](https://arxiv.org/abs/2207.08638).
- [28] R. H. Cyburt, B. D. Fields, K. A. Olive and E. Skillman, *New BBN limits on physics beyond the standard model from ${}^4\text{He}$* , *Astropart. Phys.* **23**, 313 (2005), doi:[10.1016/j.astropartphys.2005.01.005](https://doi.org/10.1016/j.astropartphys.2005.01.005), [astro-ph/0408033](https://arxiv.org/abs/astro-ph/0408033).
- [29] N. Aghanim *et al.*, *Planck 2018 results. VI. Cosmological parameters*, *Astron. Astrophys.* **641**, A6 (2020), doi:[10.1051/0004-6361/201833910](https://doi.org/10.1051/0004-6361/201833910), [Erratum: *Astron. Astrophys.* 652, C4 (2021)], [1807.06209](https://arxiv.org/abs/1807.06209).
- [30] A. Ringwald, J. Schütte-Engel and C. Tamarit, *Gravitational Waves as a Big Bang Thermometer*, *JCAP* **03**, 054 (2021), doi:[10.1088/1475-7516/2021/03/054](https://doi.org/10.1088/1475-7516/2021/03/054), [2011.04731](https://arxiv.org/abs/2011.04731).
- [31] K. Kajantie, M. Laine, K. Rummukainen and M. E. Shaposhnikov, *Is there a hot electroweak phase transition at $m_H \gtrsim m_W$?*, *Phys. Rev. Lett.* **77**, 2887 (1996), doi:[10.1103/PhysRevLett.77.2887](https://doi.org/10.1103/PhysRevLett.77.2887), [hep-ph/9605288](https://arxiv.org/abs/hep-ph/9605288).
- [32] M. B. Hindmarsh, M. Lüben, J. Lumma and M. Pauly, *Phase transitions in the early universe*, *SciPost Phys. Lect. Notes* **24**, 1 (2021), doi:[10.21468/SciPostPhysLectNotes.24](https://doi.org/10.21468/SciPostPhysLectNotes.24), [2008.09136](https://arxiv.org/abs/2008.09136).
- [33] V. Mukhanov, *Physical Foundations of Cosmology*, Cambridge University Press, Oxford, ISBN 978-0-521-56398-7, doi:[10.1017/CBO9780511790553](https://doi.org/10.1017/CBO9780511790553) (2005).
- [34] T. W. B. Kibble, *Topology of Cosmic Domains and Strings*, *J. Phys. A* **9**, 1387 (1976), doi:[10.1088/0305-4470/9/8/029](https://doi.org/10.1088/0305-4470/9/8/029).
- [35] W. Buchmuller, V. Domcke and K. Schmitz, *Spontaneous B-L Breaking as the Origin of the Hot Early Universe*, *Nucl. Phys. B* **862**, 587 (2012), doi:[10.1016/j.nuclphysb.2012.05.001](https://doi.org/10.1016/j.nuclphysb.2012.05.001), [1202.6679](https://arxiv.org/abs/1202.6679).
- [36] J. J. Blanco-Pillado, K. D. Olum and B. Shlaer, *The number of cosmic string loops*, *Phys. Rev. D* **89**(2), 023512 (2014), doi:[10.1103/PhysRevD.89.023512](https://doi.org/10.1103/PhysRevD.89.023512), [1309.6637](https://arxiv.org/abs/1309.6637).
- [37] J. Preskill and A. Vilenkin, *Decay of metastable topological defects*, *Phys. Rev. D* **47**, 2324 (1993), doi:[10.1103/PhysRevD.47.2324](https://doi.org/10.1103/PhysRevD.47.2324), [hep-ph/9209210](https://arxiv.org/abs/hep-ph/9209210).
- [38] W. Buchmuller, V. Domcke, H. Murayama and K. Schmitz, *Probing the scale of grand unification with gravitational waves*, *Phys. Lett. B* **809**, 135764 (2020), doi:[10.1016/j.physletb.2020.135764](https://doi.org/10.1016/j.physletb.2020.135764), [1912.03695](https://arxiv.org/abs/1912.03695).
- [39] W. Buchmuller, V. Domcke and K. Schmitz, *Stochastic gravitational-wave background from metastable cosmic strings*, *JCAP* **12**(12), 006 (2021), doi:[10.1088/1475-7516/2021/12/006](https://doi.org/10.1088/1475-7516/2021/12/006), [2107.04578](https://arxiv.org/abs/2107.04578).
- [40] D. Baumann, *Inflation*, In *Theoretical Advanced Study Institute in Elementary Particle Physics: Physics of the Large and the Small*, pp. 523–686, doi:[10.1142/9789814327183_0010](https://doi.org/10.1142/9789814327183_0010) (2011), [0907.5424](https://arxiv.org/abs/0907.5424).
- [41] M. C. Guzzetti, N. Bartolo, M. Liguori and S. Matarrese, *Gravitational waves from inflation*, *Riv. Nuovo Cim.* **39**(9), 399 (2016), doi:[10.1393/ncr/i2016-10127-1](https://doi.org/10.1393/ncr/i2016-10127-1), [1605.01615](https://arxiv.org/abs/1605.01615).

- [42] J. L. Cook and L. Sorbo, *Particle production during inflation and gravitational waves detectable by ground-based interferometers*, Phys. Rev. D **85**, 023534 (2012), doi:[10.1103/PhysRevD.85.023534](https://doi.org/10.1103/PhysRevD.85.023534), [Erratum: Phys.Rev.D 86, 069901 (2012)], [1109.0022](https://arxiv.org/abs/1109.0022).
- [43] K. Martinovic, C. Badger, M. Sakellariadou and V. Mandic, *Searching for parity violation with the LIGO-Virgo-KAGRA network*, Phys. Rev. D **104**(8), L081101 (2021), doi:[10.1103/PhysRevD.104.L081101](https://doi.org/10.1103/PhysRevD.104.L081101), [2103.06718](https://arxiv.org/abs/2103.06718).
- [44] V. Domcke, V. Guidetti, Y. Welling and A. Westphal, *Resonant backreaction in axion inflation*, JCAP **09**, 009 (2020), doi:[10.1088/1475-7516/2020/09/009](https://doi.org/10.1088/1475-7516/2020/09/009), [2002.02952](https://arxiv.org/abs/2002.02952).
- [45] N. Barnaby, E. Pajer and M. Peloso, *Gauge Field Production in Axion Inflation: Consequences for Monodromy, non-Gaussianity in the CMB, and Gravitational Waves at Interferometers*, Phys. Rev. D **85**, 023525 (2012), doi:[10.1103/PhysRevD.85.023525](https://doi.org/10.1103/PhysRevD.85.023525), [1110.3327](https://arxiv.org/abs/1110.3327).